Bioorganic Chemistry 103 (2020) 104191

Contents lists available at ScienceDirect

Bioorganic Chemistry

journal homepage: www.elsevier.com/locate/bioorg

Synthesis and biological evaluation of substituted *N*-(2-(1*H*-benzo[*d*]imidazol-2-yl)phenyl)cinnamides as tubulin polymerization inhibitors

Kavitha Donthiboina[a], Pratibha Anchi[b], Sowmyasree Gurram[b], Geeta Sai Mani[a], Jaya Lakshmi Uppu[a], Chandraiah Godugu[b,*], Nagula Shankaraiah[a,*], Ahmed Kamal[a,c,*]

[a] Department of Medicinal Chemistry, National Institute of Pharmaceutical Education and Research (NIPER), Hyderabad 500 037, India
[b] Department of Regulatory Toxicology, National Institute of Pharmaceutical Education and Research (NIPER), Hyderabad 500 037, India
[c] School of Pharmaceutical Education and Research (SPER), Jamia Hamdard, New Delhi 110062, India

ARTICLE INFO

Keywords:
Benzimidazole
Apoptosis
Cytotoxicity
Colchicine binding site
Flow cytometry
Reactive oxygen species
Cell migration
Molecular modeling

ABSTRACT

A new series of *N*-(2-(1*H*-benzo[*d*]imidazol-2-yl)phenyl) cinnamides was prepared and evaluated for their *in vitro* cytotoxic activity using various cancer cell lines viz. A549 (human non-small cell lung cancer), MDA-MB-231 (human triple negative breast cancer), B16-F10 (mouse melanoma), BT-474 (human breast cancer), and 4 T1 (mouse triple negative breast cancer). In the series of tested compounds, **12h** showed potent cytotoxic activity against non-small cell lung cancer cell line with IC_{50} value of 0.29 ± 0.02 μM. The cytoxicity of most potent compound **12h** was also tested on NRK-52E (normal rat kidney epithelial cell line) and showed less cytotoxicity compared to cancer cells. Tubulin polymerization assay indicated that the compound **12h** was able to impede the cell division by inhibiting tubulin polymerization. Moreover, molecular docking study also suggested the binding of **12h** at the colchicine-binding site of the tubulin protein. Cell cycle analysis revealed that the compound **12h** arrests G2/M phase. In addition, **12h** induced apoptosis in A549 cell lines was evaluated by various staining studies like acridine orange, DAPI, analysis of mitochondrial membrane potential, annexin V-FITC, and DCFDA assays.

1. Introduction

Microtubules are crucial elements of cytoskeleton composed of α-β-tubulin heterodimers [1]. They possess a significant role in modulating cellular activities such as mitosis, preserving cell structure, cell signaling and intracellular transport [2]. Dynamic instability of these filaments contribute a decisive role in the spindle formation during mitosis [3]. Hence, microtubules serve as effective target for various anti-mitotic agents. Tubulin binding agents can be categorized based on the binding site such as laulimalide, taxane/epothilone, vinca alkaloid and colchicine sites [4]. Small molecules like colchicine (**1**), combretastatin A-4 (**2**), nocodazole (**3**), E7010 (**4**) and HMN-241 (**5**, Fig. 1) interact with the colchicine binding site of tubulin. These molecules disturb microtubule formation by inhibiting tubulin assembly [5]. Over the past decade, various molecules were designed to affect tubulin dynamics [6]. Most of the studies revealed that planar or biaryl configuration is the required feature for the molecules to bind at the colchicine binding site [7].

Cinnamic acids are widely distributed as natural substances having broad spectrum of pharmacological activities such as antioxidant, anti-inflammatory, antitumor, cytoprotective, antimicrobial and tyrosinase inhibition [8]. Anti-mutagenesis property of cinnamic acid is due to its ability to interact with cellular nucleophiles such as glutathione (GSH) and cysteine. The presence of α,β-unsaturated carbonyl moiety is responsible for the cellular interactions [9]. Various reports proved the antimitotic activity of cinnamides [10]. 2-Methyl cinnamide (**6**), cinnamic mustard derivative of distamycin A (PNU-157911, **7**, Fig. 1) are the congeners of the cinnamic acid noted with anticancer activity [11]. Hence, cinnamic acid and its derivatives serve as fascinating moieties to develop new molecules with anticancer property. On the other hand, benzimidazole is a noteworthy and potent pharmacophore with various activities like anti-inflammatory, antibacterial, antiviral, anti-proliferative, H_3 receptor-antagonistic, anti-hypertensive, anthelmintic, antifungal, anti-HIV, and antioxidant [12]. Benzimidazole is also an isostere of purine nucleoside, it can easily interact with biomolecules like proteins in the living system [13]. Various natural and synthetic benzimidazole derivatives are reported with remarkable anticancer activity [14]. Nocodazole (**3**) and HOECHST 33,258 (**8**) with

* Corresponding authors at: Department of Medicinal Chemistry, National Institute of Pharmaceutical Education and Research (NIPER), Hyderabad 500 037, India (A. Kamal).
E-mail addresses: chandra.niperhyd@gov.in (C. Godugu), shankar@niperhyd.ac.in (N. Shankaraiah), ahmedkamal@iict.res.in (A. Kamal).

https://doi.org/10.1016/j.bioorg.2020.104191
Received 24 January 2020; Received in revised form 15 July 2020; Accepted 17 August 2020
Available online 26 August 2020

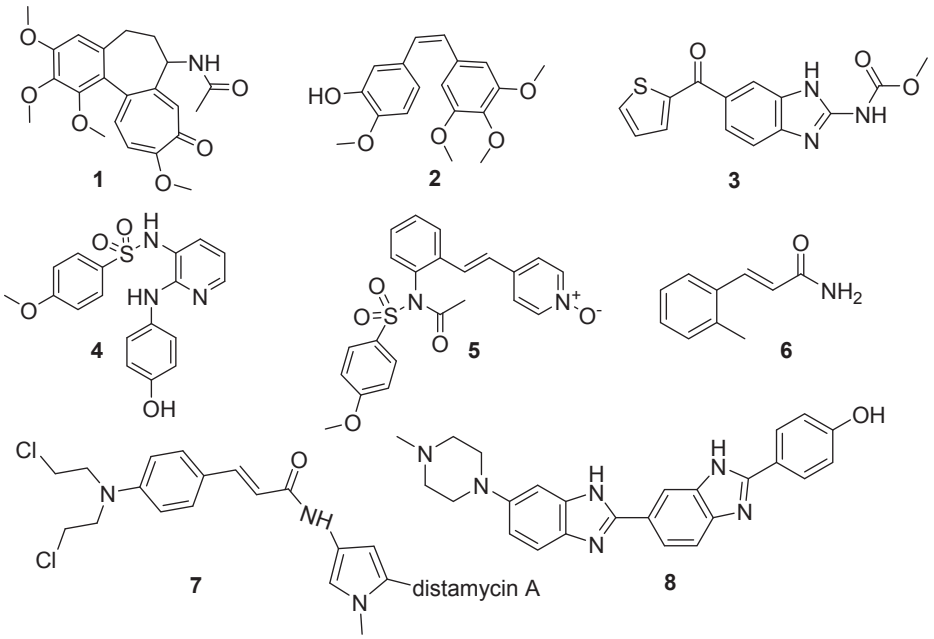

Fig. 1. Representative bioactive molecules possessing anticancer activity by inhibiting tubulin.

benzimidazole moiety (Fig. 1) are well-known antineoplastic agents.

Over the past decade, rational drug design has given emphasis to hybrids of different pharmacophoric units owing to their effect on multiple targets and improved affinity when compared to individual scaffolds [15]. In continuation of our interest to develop new anticancer molecules by molecular hybridization approach [16], herein we attempted to develop new hybrids of benzimidazole and cinnamic acid (Fig. 2) resulted with *N*-(2-(1*H*-benzo[*d*]imidazol-2- yl)phenyl)cinnamides **12a–v** and further screened for their *in vitro* cytotoxic activity.

2. Results and discussion

2.1. Chemistry

Strategy for the synthesis of *N*-(2-(1*H*-benzo[*d*] imidazol-2-yl) phenyl)cinnamides **12a–v** depicted in Scheme 1. This synthesis was initiated by the treatment of different substituted *ortho*-amino anilines **10a–e** with isatoic anhydride (**9**) in the presence of acetic acid affords the key intermediates **11a–e**. The coupling of variously substituted cinnamic acids **11f–k** with 2-(1*H*-benzo[*d*]imidazol-2-yl)anilines **11a–e** by using EDCI and HOBt in DMF resulted the desired compounds **12a–v** in excellent yields. All the synthesized compounds were confirmed by NMR spectroscopy and HRMS. In ^{1}H NMR of **12a**, the characteristic amide proton was observed at δ 13.21 ppm and sharp singlet of N—H was observed at δ 13.48 ppm. Remaining protons were observed in the range of 8.90–6.94 ppm. In ^{13}C NMR of **12a**, the carbonyl carbon was observed at δ 164.4 ppm, remaining signals appeared between δ 151.4 to 116.0 ppm. All the compounds **12a–v** showed similar pattern of signals in ^{1}H as well as in ^{13}C NMR spectra. HRMS of all the compounds showed characteristic $[M+H]^{+}$ peak equivalent to their molecular formulae.

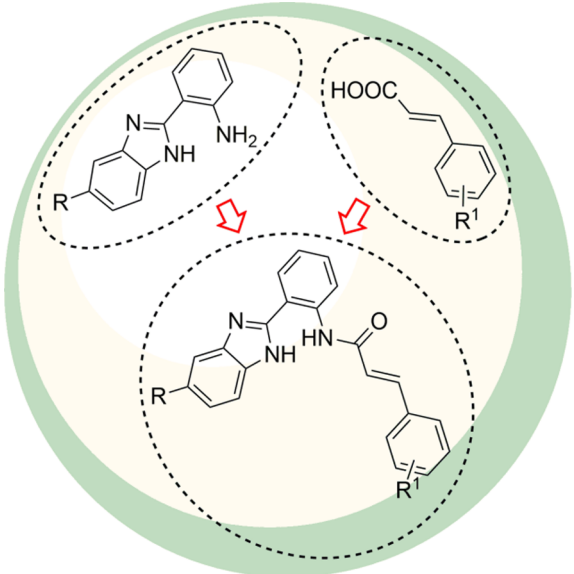

Fig. 2. Design of new *N*-(2-(1*H*-benzo[*d*]imidazol-2-yl)phenyl)cinnamides *via* molecular hybridization approach.

2.2. Biological evaluation

2.2.1. Cytotoxic activity

Compounds **12a–v** were screened for their *in vitro* cytotoxic potential by dimethylthiazol-2-yl)-2,5-diphenyltetrazolium bromide (MTT) assay [17] against a panel of tumor cell lines viz. A549 (human non-small cell lung cancer), MDA-MB-231 (human triple negative breast cancer), B16-F10 (mouse melanoma), BT-474 (human breast cancer), and 4 T1 (mouse triple negative breast cancer). Preliminary screening was performed for the compounds at 30 μM concentration, where the compounds exhibited > 50% inhibition of cell viability (IC_{50}) was further selected to generate dose response curve (DRC). The obtained IC_{50} values were compared with standard nocodozole as shown in Table 1. However, the safety of the active compound was also evaluated in normal rat kidney epithelial cell line (NRK-52E). From the Table 1, it can be inferred that around 30% of compounds i.e., **12b**, **12d**, **12h**, **12j**, **12 k**, **12 l**, **12n**, **12p, 12u** and **12v** exhibited moderate to potent cytotoxic activity, amongst which **12h** showed most potent cytotoxic activity with IC_{50} values ranging from 0.2 to 1.5 μM on different cancer cell lines.

Structure activity relationship (SAR) of this new series was exemplified by the potency based on diversified substitution on the phenyl ring of cinnamic acid as well as phenyl ring of benzimidazole (Fig. 3). The results suggest that presence of electron donating group at

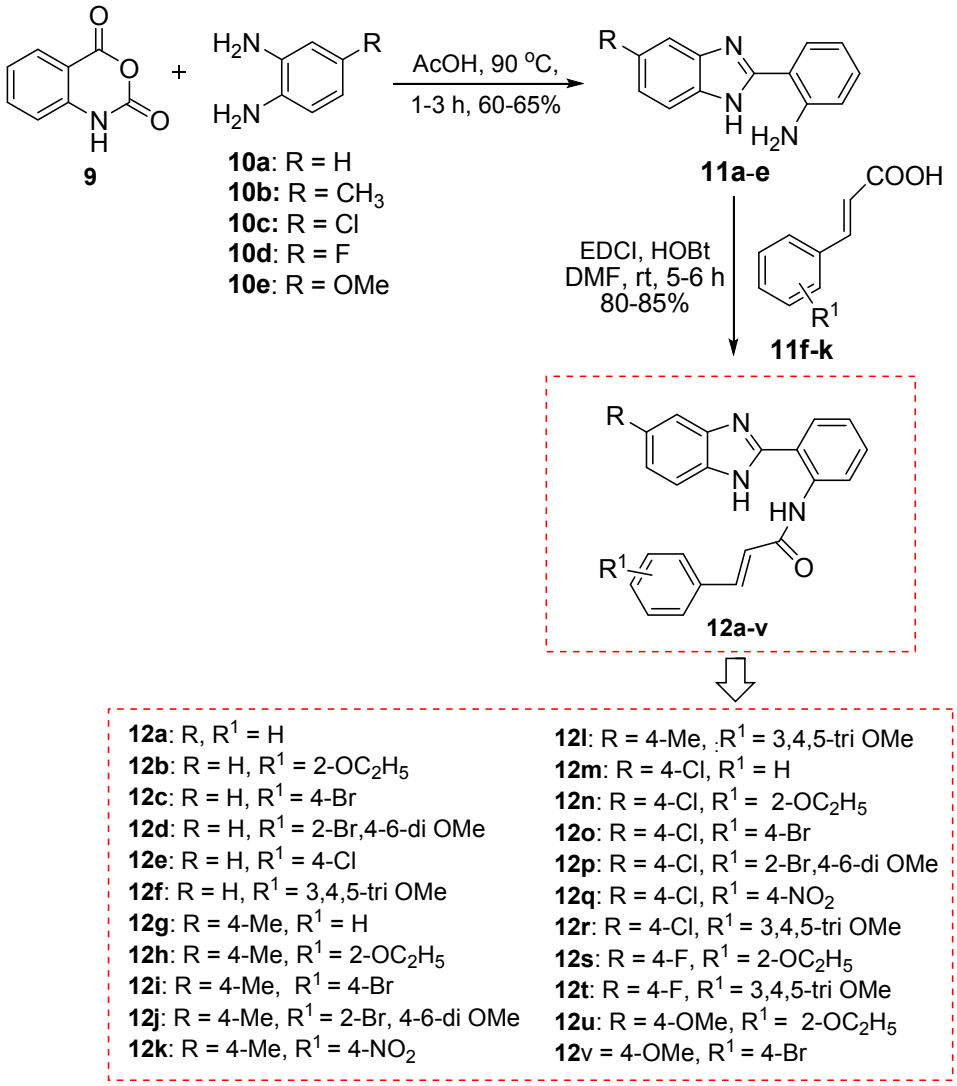

Scheme 1. Synthetic strategy for *N*-(2-(1*H*-benzo[*d*] imidazol-2- yl)phenyl)cinnamides **12a-v**.

A and B rings are responsible for the activity. Compounds **12 s–t** having F group on the A ring are less potent and showing IC_{50} values > 30 μM. Similarly, the presence of Cl group on the A ring also diminished the activity (**12n** and **12p**), apart from that **12 m**, **12o**, **12q** having electron with-drawing groups on both rings made less active on all the tested cancer cell lines.

Compounds **12b** and **12d** showed moderate cytotoxicity against all the tested cancer cell lines with IC_{50} values ranging from 3.4 to 21.7 μM, this is due to the presence of electron donating groups on B ring, whereas **12a**, **12c**, and **12e** having no substitution on A ring and electron deficient groups on B ring leads to loss of activity. Interestingly, **12j–l** and **12u-v** having methyl and methoxy substitution respectively on A ring have shown significant activity. Furthermore, **12h** having methyl group on A ring and 2-ethoxy on B ring was potent with remarkable cytotoxicity against the cancer cell lines A549 (0.29 ± 0.02 μM), MDA-MB-231 (1.48 ± 0.020 μM), B16-F10 (1.25 ± 0.04 μM), BT-474 (0.42 ± 0.10 μM), and 4 T1 (0.49 ± 0.14 μM). The conclusions from the SAR analysis revealed based on IC_{50} values, it depicts that no substitution on the phenyl ring of cinnamides **12a**, **12 g**, **12 m** and **12 s** resulted in loss of activity. In addition, the presence of electron deficient groups (F, Cl, Br and NO_2) on at least one of the phenyl (benzimidazole or cinnamide) ring leads to show lowering or loss of activity. Electron rich substitution on either of the rings resulted in moderate to good activity, except for the compounds **12f** and **12r** which have 3,4,5-tri OMe substitution on phenyl ring of cinnamide diminished the activity, this might be due to the steric hindrance.

Finally, the compound **12h** was selected as the lead compound as it has shown greater potency than standard nocodazole against the tested tumor cell lines and was further evaluated its effect on normal cells NRK-52E, the results showed less cytotoxicity (1.58 ± 0.43 μM) compared to cancer cells. With these encouraging results, we further investigated the activity of **12h** at cellular level on A549 cells.

2.2.2. Evaluation of cell morphology

Morphological examination of the cancer cell line A549 upon treatment with the compound **12h** was performed. Cells were treated with 0.1, 0.25, 0.5 μM concentrations of compound **12h**. Cells were examined and images were captured using phase contrast microscope. From Fig. 4, it is clearly observed that by increasing the concentration of the compound **12h** there was distinct loss of viable cells compared to control with a significant morphological changes and cell detachment.

2.2.3. Acridine orange staining

While developing the new anti-neoplastic agents, apoptosis induction is considered as preferable property [18]. Hence, extent of apoptosis induced by the active compound **12h** was evaluated by Acridine orange (AO) staining. Acridine orange a fluorescent dye, stains nuclei

Table 1
In vitro cytotoxic (IC_{50} value in μM)[a] activity of the synthesized compounds **12a–v.**

Compound	A549[b]	MDA-MB-231[c]	B16-F10[d]	BT-474[e]	4T1[f]	NRK-523[g]
12a	> 30	> 30	> 30	> 30	> 30	–
12b	6.37 ± 0.11	7.37 ± 0.18	5.25 ± 1.69	21.73 ± 0.59	4.14 ± 0.18	–
12c	> 30	> 30	> 30	> 30	> 30	–
12d	3.43 ± 0.23	6.97 ± 0.27	21.32 ± 0.98	11.42 ± 1.13	11.13 ± 2.69	–
12e	> 30	> 30	> 30	> 30	> 30	–
12f	> 30	> 30	> 30	> 30	> 30	–
12g	> 30	> 30	> 30	> 30	> 30	–
12h	0.29 ± 0.02	1.48 ± 0.02	1.25 ± 0.04	0.42 ± 0.10	0.49 ± 0.14	1.58 ± 0.43
12i	> 30	> 30	> 30	> 30	> 30	–
12j	2.60 ± 0.19	1.95 ± 0.17	8.57 ± 2.52	0.65 ± 0.00	1.68 ± 0.97	–
12k	4.78 ± 0.09	4.32 ± 0.12	20.09 ± 4.18	14.58 ± 0.16	7.90 ± 1.48	–
12l	18.02 ± 0.26	25.75 ± 3.73	24.59 ± 0.41	23.85 ± 1.09	2.81 ± 0.68	–
12m	> 30	> 30	> 30	> 30	> 30	–
12*n*	7.25 ± 0.58	2.18 ± 0.11	2.08 ± 0.99	14.44 ± 1.54	6.02 ± 1.27	–
12o	> 30	> 30	> 30	> 30	> 30	–
12p	8.98 ± 2.06	7.94 ± 1.76	13.37 ± 2.75	12.47 ± 0.50	26.45 ± 1.63	–
12q	> 30	> 30	> 30	> 30	> 30	–
12r	> 30	> 30	> 30	> 30	> 30	–
12s	> 30	> 30	> 30	> 30	> 30	–
12t	> 30	> 30	> 30	> 30	> 30	-
12u	1.99 ± 0.46	0.51 ± 0.09	1.87 ± 0.06	1.53 ± 0.05	1.71 ± 0.08	4.42 ± 0.30
12v	4.42 ± 3.13	5.24 ± 1.78	3.87 ± 1.29	5.12 ± 0.33	5.77 ± 1.50	4.57 ± 0.81
Nocodazole	4.44 ± 0.12	2.15 ± 0.02	1.50 ± 0.05	2.70 ± 0.08	Nd	–

[a] Concentration required for half maximal inhibition mean ± SEM of three individual experiments performed in triplicate. [b]Human non-small cell lung cancer cell line. [c]Human triple negative breast cancer cell line. [d]Mouse melanoma cell line. [e]Human breast cancer cell line. [f]Mouse triple negative breast cancer cell line. [g]Normal rat kidney epithelial cell line. Nd: Not determined.

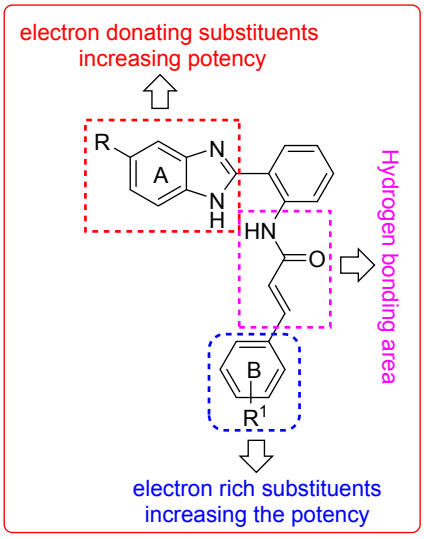

Fig. 3. SAR analysis for anticancer activity of compounds **12a–v**.

green in color by diffusing through intact cell membrane. From the Fig. 5, it can be implied that control cells exhibited normal morphology whereas the compound **12h** treated A549 cells have shown sign of early apoptosis such as rounding of the cells (change in actual morphology of cell) with lowest dose (0.1 μM). However, with increase in dose (0.25, 0.5 μM) cornering of nuclei (displacement of nuclei from the centre), formation of micronuclei was observed and represented in Fig. 5.

2.2.4. DAPI staining

DAPI (4′,6-Diamidino-2-phenyl indole) is a fluorescent nuclear stain that can bind A-T rich sequence of minor grove of DNA by which it can detect nuclear morphological changes [19]. DAPI stains apoptotic cell in bright color due to condensed nucleus, therefore DAPI staining was performed to detect apoptosis induced by the compound **12h** on the cancer cell line A549. From Fig. 6, it was observed that compound **12h** treated cells were stained bright with fragmented, horse shoe shaped

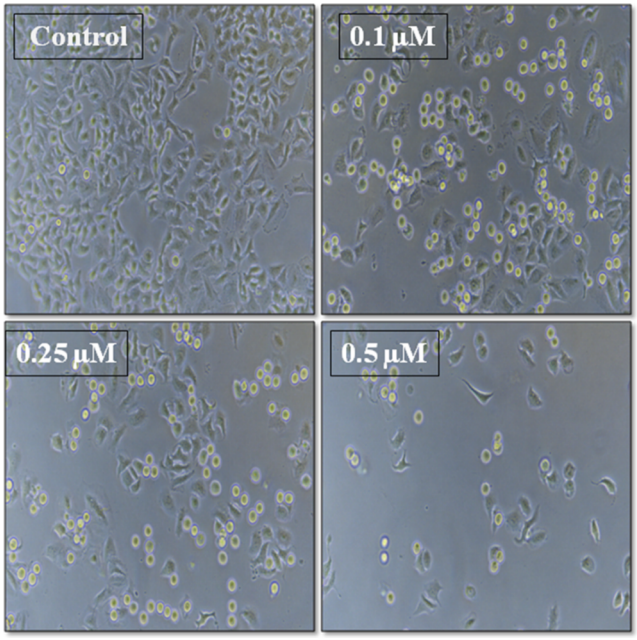

Fig. 4. Phase contrast images of A549 cells after 24 h treatment with different concentrations of compound **12 h** and compound induced morphological changes were observed at 200X magnification.

nuclei in a dose dependent manner where as control cells posses intact nuclei.

2.2.5. Measurement of reactive oxygen species by DCFDA staining

Intrinsic apoptotic cascade initiates the raise in reactive oxygen species (ROS) through oxidative damage of mitochondrial membrane, collapse of membrane potential [20]. 2′,7′–Dichlorofluorescein diacetate (DCFDA), a fluorescent dye itself converts into non-fluorescent compound by cellular esterases and further oxidized to highly fluorescent DCF by ROS generated within the cell. The extent of fluorescence depends upon amount of ROS generated. Therefore, DCFDA assay was

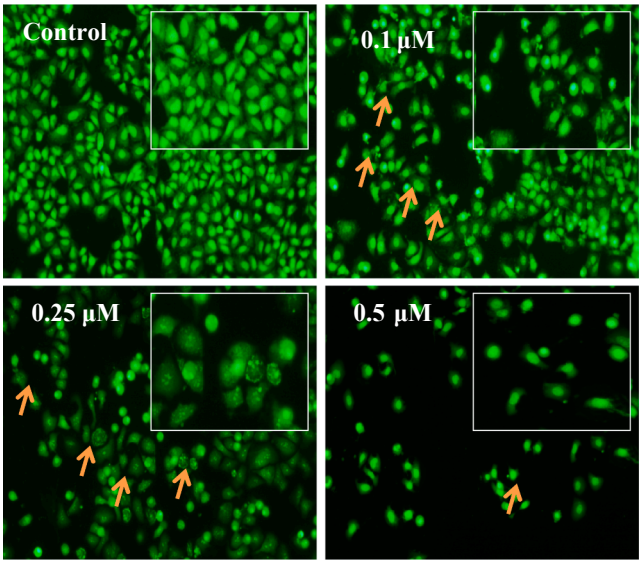

Fig. 5. Non-small cell lung cancer cells were treated for 24 h with different concentrations of compound **12 h** and stained with Acridine Orange. Apoptotic characteristics and less number of viable cells (highlighted with orange arrows) were noticed at 200X magnification. (For interpretation of the references to color in this figure legend, the reader is referred to the web version of this article.)

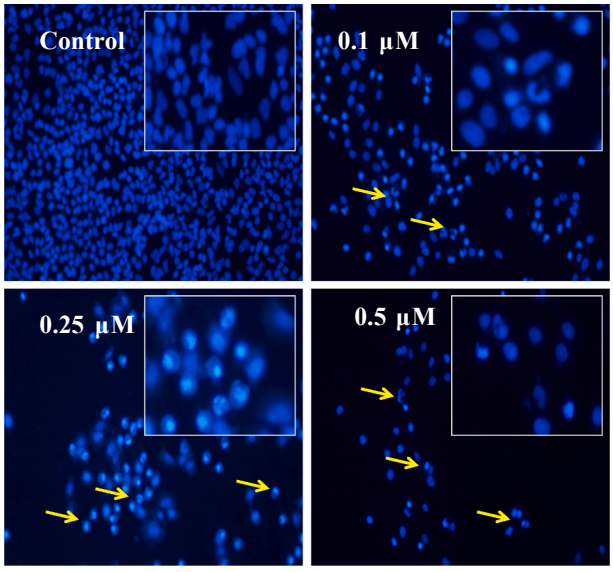

Fig. 6. DAPI staining to evaluate the morphology of nucleus. A549 cells were treated with 0.1, 0.25, 0.5 µM concentrations of compound **12 h** for 24 h and images were captured using fluorescence microscope. Appoptotic parameters highlighted with yellow arrows. (For interpretation of the references to color in this figure legend, the reader is referred to the web version of this article.)

performed to evaluate the potency of the active compound **12h** to induce ROS. From the Fig. 7, it was observed that when the cancer cell line A549 was treated with compound **12h**, there was an increase in generation of ROS (from increased fluorescence of 88.80 to 200.15 at 480/535 nm dose dependently) which was evident with the generated fluorescence in comparison to control cells. This concludes that the compound **12h** was able to induce apoptosis by the generation of ROS.

2.2.6. Effect on mitochondrial membrane potential (ΔΨm)

Mitochondria are cellular sources of energy, plays crucial role in the process of apoptotic events. Loss of mitochondrial membrane integrity by the oxidative damage due to increased ROS and dissipation of mitochondrial membrane potential is the process that occur during apoptosis [21]. Thus, effect of the compound **12h** on mitochondrial membrane potential was measured using lipophilic JC1 dye [22]. Normal polarized mitochondria possesses J aggregates and emits red to orange colour fluorescence, whereas J monomers present in depolarized mitochondria exhibits green colour fluorescence. From Fig. 8, it was clear that there was a increase in depolarized cells (*P*2 population) in a dose dependent manner, when A549 cells treated with compound **12h** at 0.1, 0.25, 0.5 µM concentrations for 24**h** and stained with JC1 dye.

2.2.7. Scratch wound healing assay

Cancerous cells have the ability to multiply and migrate throughout the body by intravasing into blood circulation, subsequently attaching to a distant site and finally extravasing by making its own identity. This invasion is currently considered as a main reason for death in cancer patients termed by metastatic progression. Hence, to evaluate the property of the compound **12h** to inhibit metastasis or cell migration, cell culture wound healing assay was performed on the A549 cell lines. It can be observed from the Fig. 9, that the % wound closure was found to be in dose dependent manner i.e., it was observed to be 36.77 ± 3.52, 11.44 ± 4.16, 6.76 ± 1.88, 4.64 ± 0.34 for control, 0.05 µM, 0.1 µM, 0.25 µM concentrations of **12h.**

2.2.8. Annexin V-FITC/Propidium iodide staining assay

Quantitative determination of the percentage of the cells undergoing apoptosis by the treatment with **12h** Annexin V-FITC/PI dual staining assay was performed. This study allows the detection of live cells (Q1-LL; AV^-/PI^-), early apoptotic cells (Q2-LR; AV^+/PI^-), late apoptotic cells (Q3-UR; AV^+/PI^+) and necrotic cells (Q4-UL; AV^-/PI^+). A549 cells were treated with 0.1, 0.2 and 0.5 µM of compound **12h** for 24**h** and stained with Annexin V-FITC/PI. From the Fig. 10, it was observed that there was increase in the percentage of late apoptotic cells [from 5.57% (control) to 27.37% (at 0.1 µM) 32.52% (at 0.25 µM) and 37.05% (at 0.5 µM)] in a dose dependent manner, which suggest that the compound **12h** induced apoptosis in A549 cells.

2.2.9. Cell cycle analysis

Most of the anticancer agents elicit cytotoxic effect either by inducing apoptosis or by inhibiting cell cycle progression [23]. To evaluate the compound **12h** induced cell cycle arrest, cell cycle analysis was performed, where A549 cells were treated with the compound **12h** at 0.1, 0.25, 0.5 µM concentrations for 24**h** and stained with propidium iodide. From the Fig. 11, it was evident that compound **12h** altering cell cycle progression profoundly. Compared to DMSO treated control cells, compound treated cells have shown more G2/M population (control: 19.5%, 0.25 µM: 29.0%, 0.5 µM: 50.3%) and less G0/G1 population (control: 49.9%, 0.25 µM: 21.2%, 0.5 µM: 4.9%), these results indicated that compound **12h** alter the cell cycle by arresting progression at G2/M phase.

2.2.10. Effect of compound on tubulin polymerization

Tubulin is an essential element for the cell replication; *in vitro* results revealed that cytotoxic effect of the compound **12h** and flow cytometric analysis proved arrest of G2/M phase of the cell cycle. To know the antimitotic activity of the compound **12h,** tubulin polymerization assay was performed, as tubulin is the critical element in the mitosis. The effect of compound **12h** on tubulin polymerization in a cell free *in vitro* tubulin assay using paclitaxel as standard at 3 µM concentration, in comparison with control groups illustrated in Fig. 12. The compound **12h** has shown inhibition of tubulin polymerization with IC_{50} value of 4.64 ± 0.09 µM

2.2.11. Molecular docking studies

Molecular docking simulation studies were performed to interpret the mode of binding and type of interactions with active site of tubulin

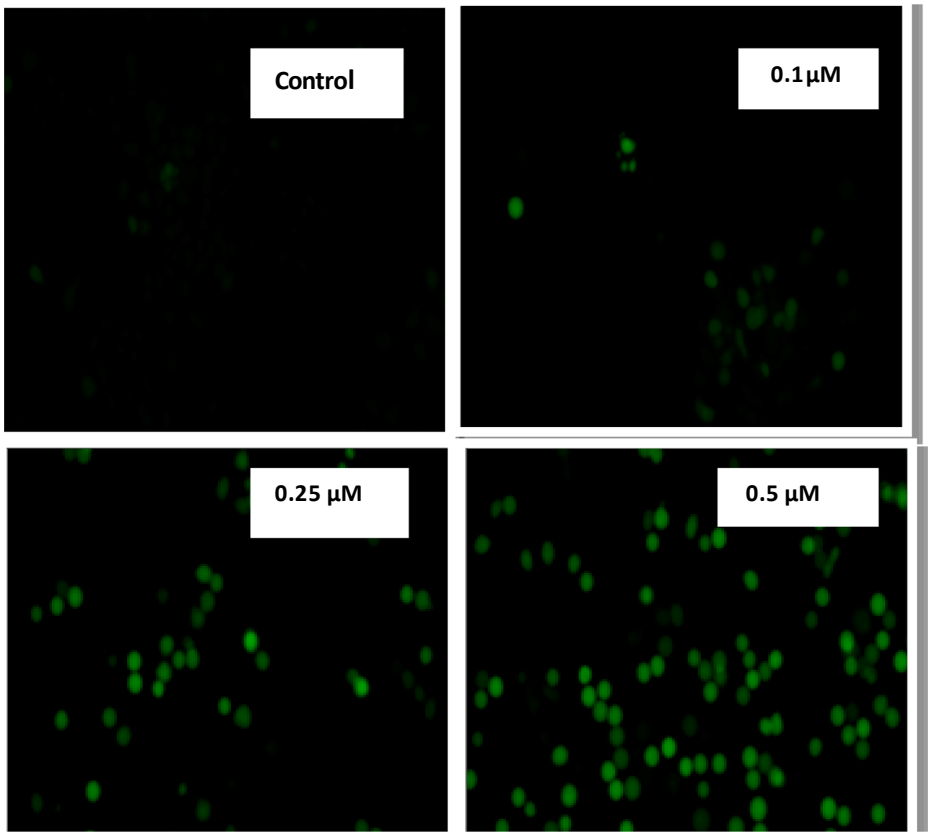

Fig. 7. DCFDA assay illustrating activity of compound **12h** on generation of ROS at concentrations 0.1, 0.25 and 0.5 µM in A549 cancer cell line after 24 h treatment.

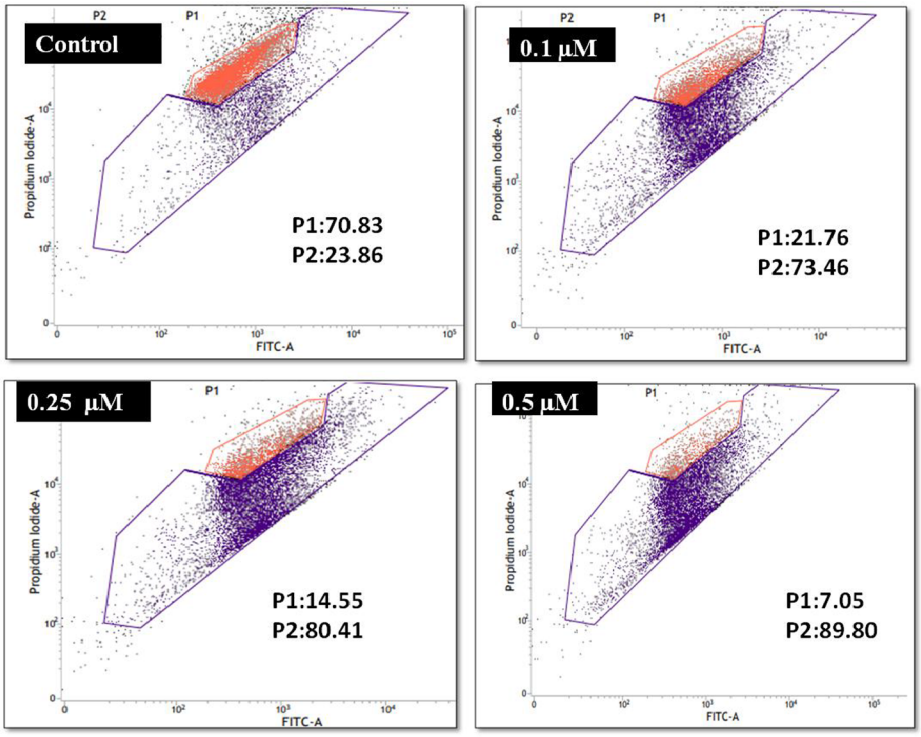

Fig. 8. Image representing ratio of J aggregates (orange colour *P*1) to J monomers (*P*2 blue colour). Fluorescence of JC-1 was analysed using Flow cytometer (BD FACSVerse™, USA). Here 10,000 events for each group was calculated for the analysis. (For interpretation of the references to color in this figure legend, the reader is referred to the web version of this article.)

(PDB ID: 3E22) [24] by using GLIDE (Grid based Ligand Docking with Energetics) docking module of Schrödinger suite 2017–1. Glide has been optimized for docking accuracy and also to dock prepared ligands in a reasonable time with the active site of a receptor [29]. This study explains that top ranked confirmation of compound **12h** bind effectively at the colchicine-binding site of the tubulin. From Fig. 13, it can be noticed that the carbonyl oxygen of amide acts as hydrogen bond acceptor in sequential hydrogen bonding with NH_2 of Asn249 (d = 3.61 Å), Ala250 (d = 3.61 Å), Asp251 (d = 3.79 Å) of colchicine binding site of tubulin, these interactions play a crucial role in binding.

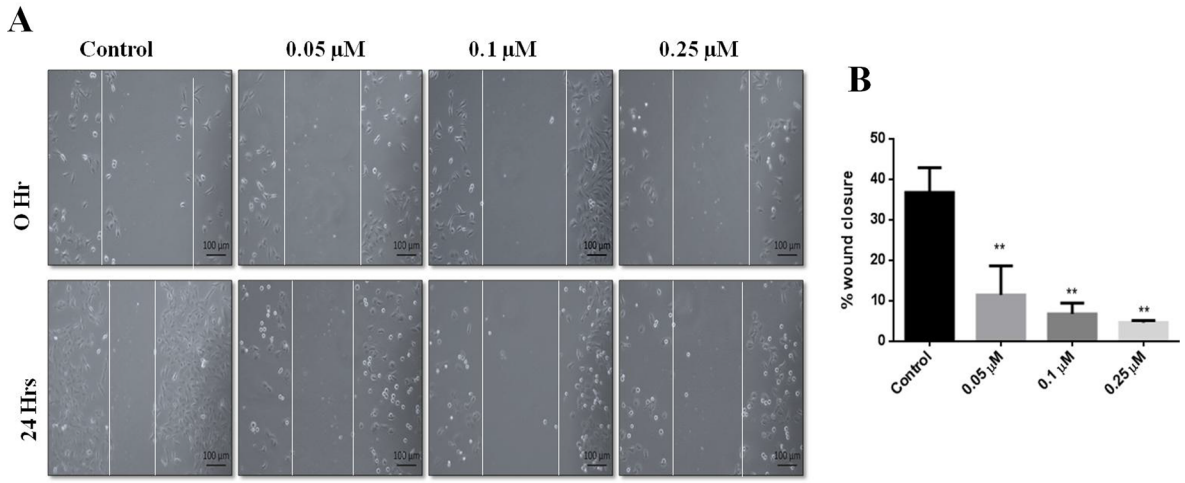

Fig. 9. A) Images of wound closure observed after 0 and 24 hrs upon treatment with compound **12 h** (at magnification 100X). B.Graph represents the calculated percentage wound closure at various doses of **12 h.** Data represented **p < 0.01 vs control. Data was analysed by one way ANOVA followed Tukeys multiple comparision.

In addition, various hydrophobic interactions were noticed with active site of amino acids, Val238, Cys241, Leu242, Leu248, Ala250, Leu252, Leu255, Met259, Val315, Ala316, Ala317, Val318, Val351, Ala354, and Ile378. These interactions stabilize the binding of potent compound **12h** to the colchicine-binding site of tubulin. Based on these observations, it can be inferred that molecular docking simulation studies proved the rationalization of tubulin inhibitory activity of most potent compound **12h**.

3. Conclusion

With an aim to develop new cytotoxic agents, a series of *N*-(2-(1*H*-benzo[*d*]imidazol-2-yl)phenyl) cinnamides **12a–v** was synthesized and well characterized. Initially, these compounds were screened for the *in vitro* cytotoxic activity using various cancer cell lines such as A549 (human non-small cell lung cancer), MDA-MB-231 (human triple negative breast cancer), B16-F10 (mouse melanoma), BT-474 (human breast), and 4 T1 (mouse triple negative breast cancer). Compound **12h**

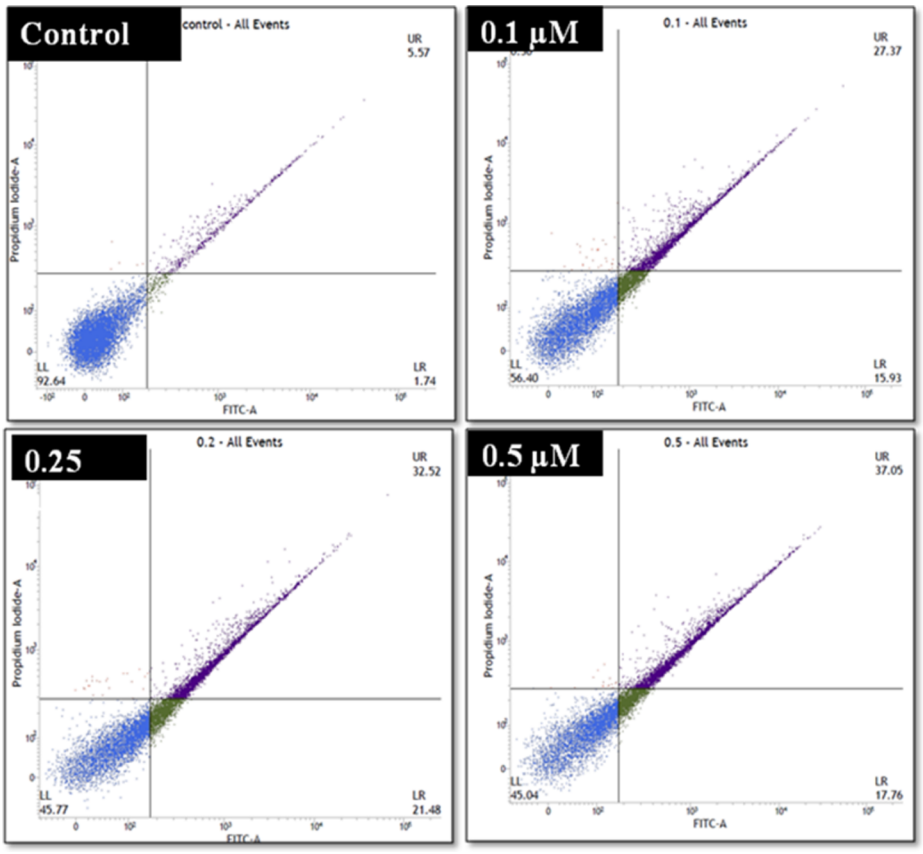

Fig. 10. Annexin V-FITC/propidium iodide (PI) dual staining assay. A549 cells were treated with different concentrations compound **12 h**, labelled with Annexin V-FITC/PI, and observed for apoptosis using flow-cytometer. Cells in the lower left quadrant (Q1-LL: AV^-/PI^-): live cells; lower right quadrant (Q2-LR: AV^+/PI^-): early apoptotic cells; upper right quadrant (Q3-UR: AV^+/PI^+): late apoptotic cells and upper left quadrant (Q4-UL: AV^-/PI^+): necrotic cells.

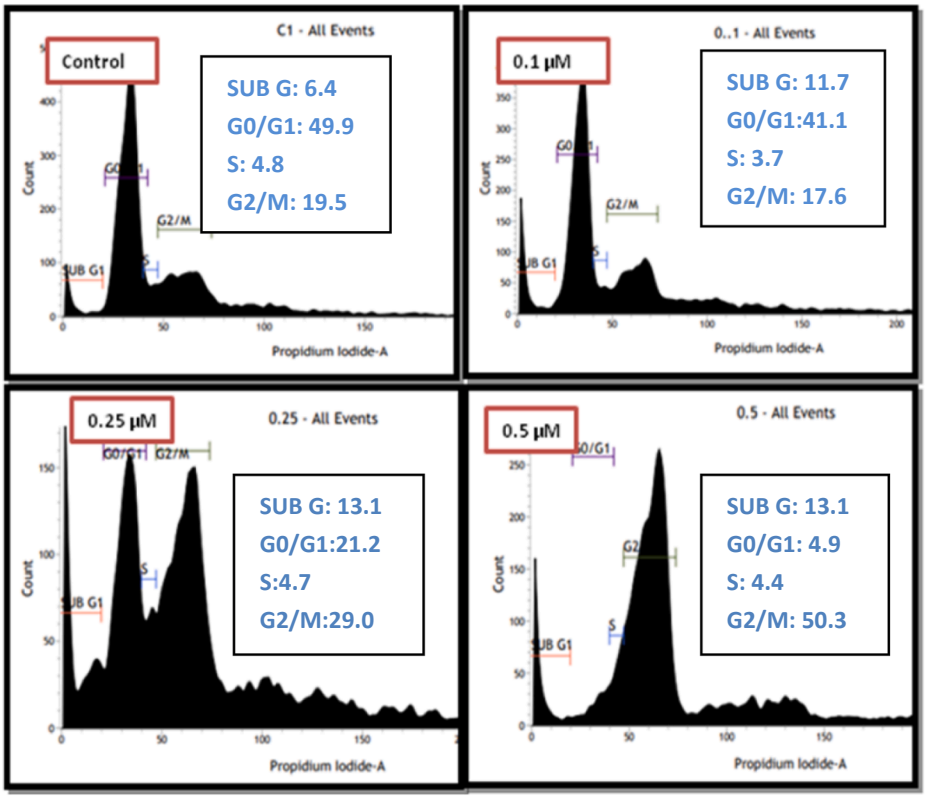

Fig. 11. Flow cytometric analysis of A549 cells by the treatment of compound **12 h**. DNA histogram represents different stages of cell cycle i.e., SubG1, G0/G1, S, G2/M. Cell cycle results of each phase of treated cells were compared with control cells.

expressed best cytotoxic potential against lung cancer cell line (A549) with an IC_{50} value of 0.29 ± 0.02 µM,. *In vitro* tubulin assay results explained that compound **12h** was able to interrupt mitosis by inhibiting tubulin polymerization and molecular docking study also supported the tubulin binding property of compound **12h**. Cell cycle analysis resulted that compound **12h** was able to arrest G2/M phase. Additional studies such as acridine orange, DAPI staining, annexin V-FITC/propidium iodide staining, analysis of mitochondrial membrane potential and ROS assays proved compound **12h** induced apoptosis. Moreover, wound healing assay proved that compound **12h** could interfere migration of tumor cells. Finally, we believe that **12h** could be the lead compound for the development of chemical library that would serve as a potential entity to treat cancer.

4. Experimental section

Commercially available starting materials, reagents and solvents were used directly without any further purification. TLC was performed on 0.25 mm silica gel 60-F_{254} plates. UV light was used to detect product formation by visualizing spots. ^{1}H and ^{13}C spectra were recorded on 500 MHz spectrometers using tetramethylsilane as internal standard. Chemical shifts were reported in parts per million (ppm) downfield from tetramethylsilane. Spin multiplicities were described as s (singlet), d (doublet), t (triplet), q (quartet), m (multiplet), dd (double doublet). Coupling constants were reported in Hertz. HRMS analyses were acquired on single quadruple and carried out using ESI technique 70 eV. All molecular formulae were mentioned by adding extra proton to represent $[M+H]^{+}$. Column chromatography was performed by using 60–120 mm silica-gel with hexane and ethyl acetate. Melting points

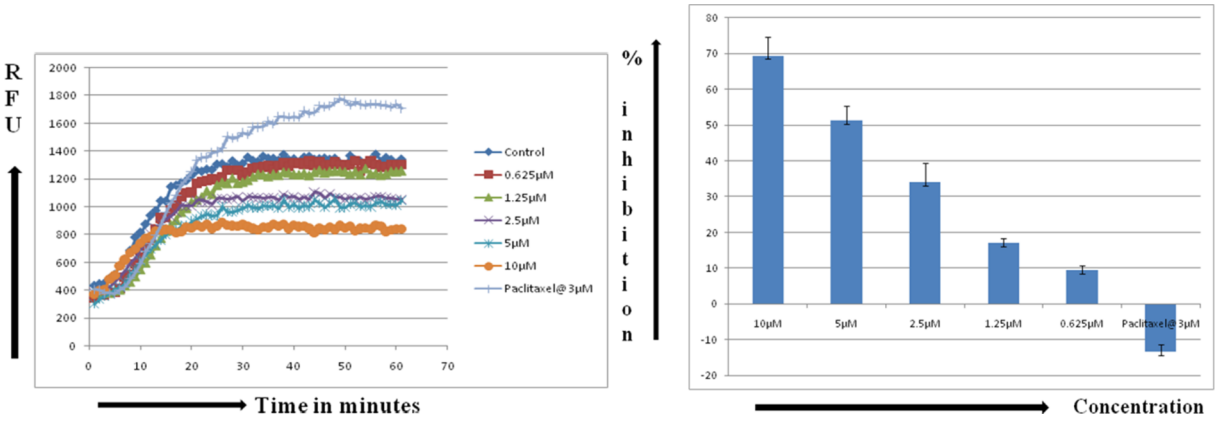

Fig. 12. Effect of compound **12 h** on tubulin polymerization.

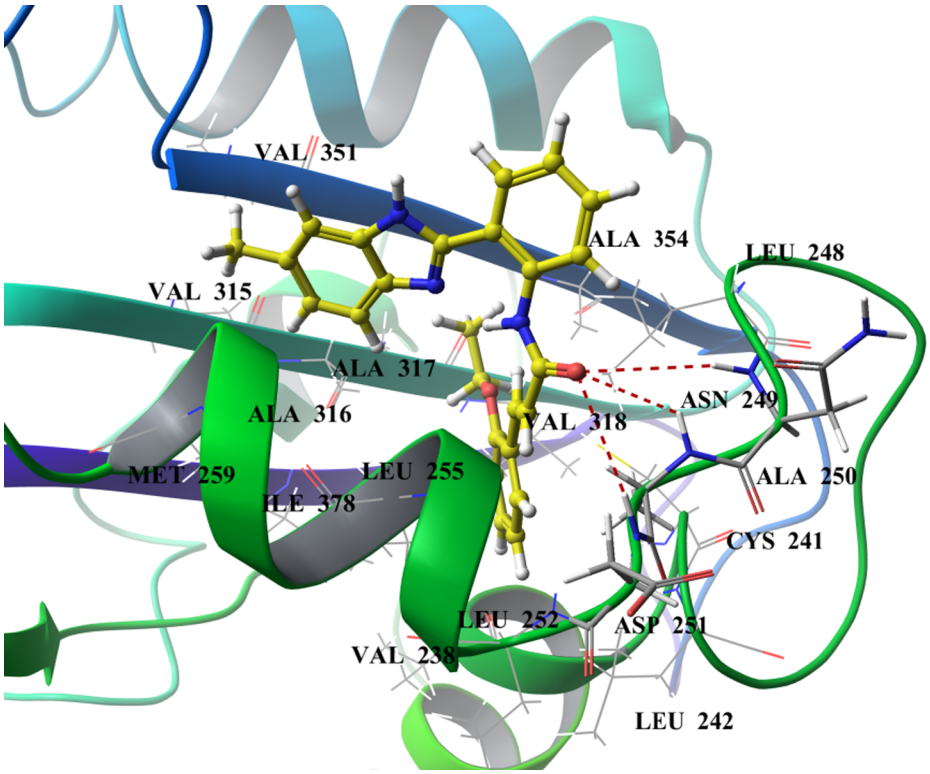

Fig. 13. Docking pose of the most active compound **12 h**. (Yellow colour ball and stick) in the colchicine-binding site of tubulin and the interacting amino acids (PDB ID: 3E22). The red dashed lines represent hydrogen bonds. (For interpretation of the references to color in this figure legend, the reader is referred to the web version of this article.)

were determined with an Electro thermal melting point apparatus and were uncorrected.

4.1. General procedure [25] to synthesize substituted 2-(1H-benzo[d] imidazol-2-yl) aniline (10a–e)

To a mixture of isatoic anhydride (**9**, 1 mmol) and *ortho*-phenylene diamine (10, 1 mmol) was added glacial acetic acid (2 mL) and allowed to stir at 90 °C for 1–3**h**, reaction was monitored by TLC. After completion of the reaction, acetic acid was evaporated. Saturated solution of $NaHCO_3$ was used to quench the reaction mixture and extracted with ethyl acetate (3x20 mL). The combined organic layers dried over anhydrous Na_2SO_4 filtered, concentrated and then purified by column chromatography using ethyl acetate and hexane (15%) as eluent to afford the corresponding 2-(1*H*-benzo[*d*]imidazol-2-yl)aniline **10a-e**.

4.2. General procedure [26] for the synthesis of substituted N-(2-(1H-benzo [d]imidazol-2-yl)phenyl)cinnamamide (12a–v)

To a stirred solution of substituted cinnamic acids **11f-k** (1 equiv.) in dry DMF (5 mL), EDCI (1.05 equiv.), HOBt (1.05 equiv), were added and stirred for 30 min at room temperature. Later, 2-(1*H*-benzo[*d*] imidazol-2-yl)aniline **11a-e** (1.05 equiv.) was added to the reaction mixture and allowed to stir at room temperature until consumption of starting material. The reaction mixture was then diluted with EtOAc (20 mL), washed with cold H_2O (2 times). The organic layer was dried over Na_2SO_4 filtered and concentrated. The resulting residue was purified by column chromatography using EtOAc/Hexane to afford the final compounds **12a-v**.

4.2.1. N-(2-(1H-Benzo[d]imidazol-2-yl)phenyl)cinnamamide (12a)

Off-white solid; Yield: 80%, 60 mg; M.p: 190–192 °C; FT-IR (cm^{-1}): 3360.5, 3014.5, 2936.5, 1740.5, 1610, 1585, 1350, 1050; ^{1}H NMR (500 MHz, DMSO-d_6): δ 13.47 (s, 1H), 13.21 (s, 1H), 8.86 (d, J = 8.3 Hz, 1H), 8.17 (d, J = 7.8 Hz, 1H), 7.82 (d, J = 6.9 Hz, 2H), 7.75 (m, 2H), 7.57–7.41 (m, 5H), 7.3–7.24 (m, 3H), 6.93 (d, J = 15.6 Hz, 1H). ^{13}C NMR (125 MHz, DMSO-d_6): δ 164.5, 151.4, 141.2, 139.0, 134.8, 131.2, 130.5, 129.5, 128.6, 127.8, 123.5, 123.3, 120.6, 116.0. HRMS (ESI): m/z calculated for $[M+H]^+$ $C_{22}H_{18}N_3O$: 340.1450 found 340.1453.

4.2.2. (E)-N-(2-(1H-Benzo[d]imidazol-2-yl)phenyl)-3-(2-ethoxyphenyl) acrylamide (12b)

Off-white solid; Yield: 82%, 65 mg; M.p: 195–198 °C; FT-IR (cm^{-1}): 3457.0, 3267.9, 3004.2, 2970.9, 2873.8, 1738.4, 1667.4, 1621.9, 1586.3, 1043.9; ^{1}H NMR (500 MHz, DMSO-d_6): δ 13.37 (s, 1H), 13.21 (s, 1H), 8.88 (d, J = 8.2 Hz, 1H), 8.16 (d, J = 7.6 Hz, 1H), 7.98 (d, J = 15.8 Hz, 1H), 7.87–7.76 (m, 2H), 7.61 (d, J = 7.3 Hz, 1H), 7.53 (t, J = 7.6 Hz, 1H), 7.42 (t, J = 7.5 Hz, 1H), 7.36–7.25 (m, 3H), 7.13 (d, J = 8.3 Hz, 1H), 7.05 (t, J = 7.3 Hz, 1H), 6.99 (d, J = 15.8 Hz, 1H), 4.20 (q, J = 13.6, 6.7 Hz, 2H), 1.45 (t, J = 6.8 Hz, 3H). ^{13}C NMR (125 MHz, DMSO-d_6): δ 164.9, 157.9, 151.46, 142.6, 139.0, 136.9, 134.00, 131.9, 131.1, 129.7, 127.9, 124.0, 123.5, 123.4, 123.3, 122.7, 121.2, 120.6, 119.1, 115.9, 113.1, 112.0, 64.4, 15.2. HRMS (ESI): m/z calculated for $[M+H]^+$ $C_{24}H_{22}N_3O_2$ 384.1712; found 384.1738.

4.2.3. (E)-N-(2-(1H-Benzo[d]imidazol-2-yl)phenyl)-3-(4-bromophenyl) acrylamide (12c)

Off-white solid; Yield: 78%, 55 mg; M.p: 272–276 °C; FT-IR (cm^{-1}): 3340.5, 3012.5, 2946.5, 1742.5, 1640, 1585, 1350, 950; ^{1}H NMR (500 MHz, DMSO-d_6): δ 13.50 (s, 1H), 13.38 (s, 1H), 8.85 (d, J = 7.6 Hz, 1H), 8.18 (s, 1H), 7.89–7.62 (m, 7H), 7.53 (s, 1H), 7.42–7.21 (m, 3H), 6.97 (d, J = 15.4 Hz, 1H). ^{13}C NMR (125 MHz, DMSO-d_6): δ 164.3, 151.3, 140.2, 140.0, 138.8, 134.2, 132.4, 131.3, 131.1, 130.7, 130.6, 127.8, 124.2, 123.7, 123.6, 120.7, 116.1. HRMS (ESI): m/z calculated for $[M+H]^+$ $C_{22}H_{17}N_3BrO$ 418.0555; found 418.0585.

4.2.4. (E)-N-(2-(1H-Benzo[d]imidazol-2-yl)phenyl)-3-(2-bromo-4,6-dimethoxyphenyl)acrylamide (12d)

Off-white solid; Yield: 75%, 60 mg; M.p: 210–213 °C; FT-IR (cm^{-1}): 3347.0, 3227.9, 3024.2, 2960.9, 2853.8, 1748.4, 1657.4, 1631.9,

1596.3, 1023.9; ^{1}H NMR (500 MHz, DMSO-d_6): δ 13.47 (s, 1H), 13.20 (s, 1H), 8.85 (d, J = 7.2 Hz, 1H), 8.21–8.12 (m, 1H), 8.02–7.82 (m, 2H), 7.74–7.49 (m, 4H), 7.38–7.23 (m, 3H), 6.96 (d, J = 15.2 Hz, 1H), 3.96 (s, 3H), 3.86 (s, 3H) ppm; ^{13}C NMR (125 MHz, DMSO-d_6): δ 168.0, 164.4, 151.8, 151.6, 151.3, 149.2, 141.9, 138.9, 138.9, 131.1, 128.3, 127.8, 127.6, 126.3, 125.8, 124.9, 124.4, 123.5, 120.8, 120.5, 119.6, 116.7, 116.5, 116.2, 116.1, 111.0, 110.7, 110.1, 56.6, 56.5. HRMS (ESI): *m/z* calcd for $[M+H]^+$ $C_{24}H_{21}Br^{81}N_3O_3$ 480.0766; found 480.0782.

4.2.5. (E)-N-(2-(1H-Benzo[d]imidazol-2-yl)phenyl)-3-(4-nitrophenyl) acrylamide (12e)

Yellow solid; Yield: 79%, 58 mg; M.p: 283–285 °C; FT-IR (cm^{-1}): 3457.0, 3016.5, 3004.2, 2970.9, 1738.4, 1668.7, 1590.4, 1349.5, 1052.4; ^{1}H NMR (500 MHz, DMSO-d_6): δ 13.60 (s, 1H), 13.23 (s, 1H), 8.85 (d, J = 7.7 Hz, 1H), 8.34–8.08 (m, 5H), 7.94 (s, 1H), 7.84 (d, J = 15.8 Hz, 1H), 7.65–7.50 (m, 2H), 7.33 (s, 3H), 7.15 (d, J = 15.7 Hz, 1H). ^{13}C NMR (125 MHz, DMSO-d_6): δ 163.6, 151.2, 148.3, 141.5, 138.8, 138.7, 131.2, 129.7, 127.8, 127.6, 124.5, 123.8, 122.7, 120.7, 119.5, 116.2, 112.0. HRMS (ESI): *m/z* calcd for $[M+H]^+$ $C_{22}H_{17}N_4O_3$ 385.1301; found 385.1320.

4.2.6. (E)-N-(2-(1H-Benzo[d]imidazol-2-yl)phenyl)-3-(3,4,5-trimethoxyphenyl)acrylamide (12f)

White solid; Yield: 80%, 62 mg; M.p: 252–255 °C; FT-IR (cm^{-1}): 3456.9, 3204.5, 3004.3, 2970.9, 1738.8, 1621.9, 1584.5, 1366.2, 1217.1, 1043.9; ^{1}H NMR (500 MHz, DMSO-d_6): δ 13.44 (s, 1H), 13.21 (s, 1H), 8.85 (d, J = 8.0 Hz, 1H), 8.17 (d, J = 7.5 Hz, 1H), 7.90 (d, J = 6.9 Hz, 1H), 7.75–7.46 (m, 4H), 7.32 (s, 2H), 7.15 (s, 2H), 6.93 (d, J = 15.8 Hz, 1H), 3.91 (s, 6H), 3.74 (s, 3H). ^{13}C NMR (125 MHz, DMSO-d_6): δ 164.7, 153.6, 151.3, 142.6, 141.5, 139.6, 139.0, 134.0, 131.2, 130.5, 127.8, 124.0, 123.5, 122.83, 122.7, 120.7, 119.3, 119.0, 115.9, 112.1, 112.00, 106.2, 60.7, 56.5. HRMS (ESI): *m/z* calcd for $[M+H]^+$ $C_{25}H_{24}N_3O_4$ 430.1767; found 430.1768.

4.2.7. N-(2-(5-Methyl-1H-benzo[d]imidazol-2-yl)phenyl)cinnamamide (12 g)

Off-white solid; Yield: 75%, 50 mg; M.p: 248–250 °C; FT-IR (cm^{-1}): 3357.0, 3026.5, 2970.9, 2960.5, 1738.4, 1669.5, 1542.3, 1317.7, 1126.4; ^{1}H NMR (500 MHz, DMSO-d_6): δ 13.51 (s, 1H), 13.05 (s, 1H), 8.86 (s, 1H), 8.15 (s, 1H), 7.99–7.16 (s, 4H), 7.63–7.36 (m, 5H), 7.34–7.08 (d, 2H), 6.93 (s, 1H), 2.50 (s, 3H). ^{13}C NMR (125 MHz, DMSO-d_6): δ 164.6, 150.7, 141.2, 138.8, 134.9, 134.2, 133.5, 130.9, 130.5, 129.5, 128.6, 127.6, 125.4, 124.3, 123.5, 123.2, 120.6, 118.9, 116.2, 111.6, 22.2. HRMS (ESI): *m/z* calcd for $[M+H]^+$ $C_{23}H_{20}N_3O$ 354.1606; found 354.1632.

4.2.8. (E)-3-(2-Ethoxyphenyl)-N-(2-(5-methyl-1H-benzo[d]imidazol-2-yl) phenyl)acrylamide (12 h)

Off-white solid; Yield: 80%, 62 mg; M.p: 200–202 °C; FT-IR (cm^{-1}): 3263.5, 2970.9, 2840.8, 1738.4, 1667.4, 1621.9, 1576.3, 1023.9; ^{1}H NMR (500 MHz, DMSO-d_6): δ 13.37 (s, 1H), 13.21 (s, 1H), 8.88 (d, J = 8.2 Hz, 1H), 8.16 (d, J = 7.6 Hz, 1H), 8.01–7.94 (m, 1H), 7.79 (d, J = 7.4 Hz, 1H), 7.70 (d, J = 8.2 Hz, 1H), 7.62 (s, 1H), 7.50 (q, J = 15.5, 7.9 Hz, 1H), 7.45–7.37 (m, 1H), 7.28 (t, J = 7.5 Hz, 1H), 7.18 – 7.10 (m, 2H), 7.07 – 7.03 (m, 1H), 6.98 (d, J = 15.8 Hz, 1H), 4.19 (q, J = 12.1, 5.6 Hz, 2H), 2.51 (s, 3H), 1.45 (t, J = 6.8 Hz, 3H). ^{13}C NMR (125 MHz, DMSO-d_6): δ 165.0, 157.9, 150.8, 143.00, 140.7, 138.8, 136.8, 134.1, 133.4, 131.8, 131.0, 129.8, 127.6, 125.4, 124.3, 123.3, 121.2, 120.6, 118.7, 116.0, 113.1, 111.6, 64.3, 21.7, 15.2. HRMS (ESI): *m/z* calcd for $[M+H]^+$ $C_{25}H_{24}N_3O_2$ 398.1869; found 398.1895.

4.2.9. (E)-3-(4-Bromophenyl)-N-(2-(5-methyl-1H-benzo[d]imidazol-2-yl) phenyl)acrylamide (12i)

Off-white solid; Yield: 70%, 50 mg; M.p: 213–215 °C; FT-IR (cm^{-1}): 3247.0, 3016.5, 2970.7, 1738.8, 1669.5, 1542.3, 1375.7, 1229.4; ^{1}H NMR (500 MHz, DMSO): δ 13.61 (s, 1H), 12.73 (s, 1H), 8.50–8.30 (m, 2H), 8.29–8.15 (m, 3H), 7.99 (d, J = 8.3 Hz, 3H), 7.95–7.78 (m, 2H), 7.75–7.66 (m, 1H), 7.43 (t, J = 13.0 Hz, 1H), 6.75 (d, J = 16.0 Hz, 1H), 2.09 (s, 3H). ^{13}C NMR (125 MHz, DMSO-d_6): δ 167.9, 164.2, 143.3, 143.0, 140.0, 138.7, 134.0, 132.4, 132.31, 130.6, 128.3, 127.7, 124.9, 124.2, 124.0, 123.7, 123.5, 120.6, 119.6, 116.1, 110.1, 21.8. HRMS (ESI): *m/z* calculated for $[M+H]^+$ $C_{23}H_{19}Br^{81}N_3O$ 434.0691; found 434.0692.

4.2.10. (E)-3-(2-Bromo-4,6-dimethoxyphenyl)-N-(2-(5-methyl-1H-benzo [d]imidazol-2-yl)phenyl)acrylamide(12j)

Off-white solid; Yield: 70%, 50 mg; M.p: 268–279 °C; FT-IR (cm^{-1}): 3265.7, 3006.5, 2970.7, 1738.8, 1669.5, 1590.7, 1433.7, 1260.2; ^{1}H NMR (500 MHz, DMSO-d_6): δ 13.52 (bs, 1H), 13.05 (bs, 1H), 8.83 (t, J = 9.4 Hz, 1H), 8.14 (d, J = 7.7 Hz, 1H), 7.93 (dd, J = 12.5, 6.7 Hz, 1H), 7.76–7.63 (m, 1H), 7.56 (s, 1H), 7.54–7.45 (m, 1H), 7.38 (s, 1H), 7.34–7.26 (m, 2H), 7.17–7.07 (m, 1H), 6.94 (d, J = 15.5 Hz, 1H), 3.96 (s, 3H), 3.85 (s, 3H), 2.44 (s, 3H). ^{13}C NMR (125 MHz, DMSO-d_6): δ 164.4, 151.6, 149.2, 149.2, 138.8, 138.8, 130.9, 127.6, 126.3, 126.1, 124.50, 124.4, 123.5, 120.7, 116.5, 116.2, 116.1, 116.0, 110.9, 110.6, 56.6, 56.4, 21.8. HRMS (ESI): *m/z* calcd for $[M+H]^+$ $C_{25}H_{23}BrN_3O_3$ 492.0923; found 492.0925.

4.2.11. (E)-N-(2-(5-Methyl-1H-benzo[d]imidazol-2-yl)phenyl)-3-(4-nitrophenyl)acrylamide (12 k)

Yellow solid; Yield: 78%, 52 mg; M.p: 211–214 °C; FT-IR (cm^{-1}): 3457.0, 3016.6, 2970.8, 1738.6, 1600.8, 1523.6, 1347.5, 1229.4; ^{1}H NMR (500 MHz, DMSO-d_6): δ 13.62 (d, J = 19.4 Hz, 1H), 13.08 (d, J = 18.4 Hz, 1H), 8.85 (d, J = 7.5 Hz, 1H), 8.31 (s, 2H), 8.24–8.06 (m 3H), 7.98 (d, J = 8.2 Hz, 1H), 7.88–7.77 (m, 2H), 7.52 (d, J = 6.8 Hz, 1H), 7.39 (s, 1H), 7.31 (s, 1H), 7.14 (d, J = 14.2 Hz, 1H), 2.49 (s, 3H). ^{13}C NMR (125 MHz, DMSO-d_6): δ 167.5, 163.7, 148.5, 148.3, 141.7, 141.5, 141.2, 138.9, 138.6, 131.0, 129.7, 128.3, 127.6, 124.8, 124.5, 124.3, 124.1, 123.7, 120.7, 119.5, 116.3, 1010.1, 21.8. HRMS (ESI): *m/z* calcd for $[M+H]^+$ $C_{23}H_{19}N_4O_3$ 399.1457; found 399.1455.

4.2.12. (E)-N-(2-(5-Methyl-1H-benzo[d]imidazol-2-yl)phenyl)-3-(3,4,5-trimethoxyphenyl) acrylamide (12 l)

White solid; Yield: 73%, 53 mg; M.p: 256–259 °C; FT-IR (cm^{-1}): 3436.5, 3106.8, 3014.3, 2960.5, 1738.6, 1621.9, 1584.5, 1366.2, 1227.1, 1053.9; ^{1}H NMR (500 MHz, DMSO-d_6): δ 13.49 (s, 1H), 13.06 (s, 1H), 8.84 (d, J = 7.4 Hz, 1H), 8.14 (d, J = 7.7 Hz, 1H), 7.72–7.65 (m, 2H), 7.51 (t, J = 7.5 Hz, 1H), 7.39 (s, 1H), 7.28 (t, J = 7.4 Hz, 1H), 7.13 (s, 3H), 6.91 (d, J = 15.6 Hz, 1H), 3.91 (s, 6H), 3.73 (s, 3H), 2.48 (s, 3H). ^{13}C NMR (126 MHz, DMSO): δ 164.7, 153.7, 150.9, 141.3, 139.7, 138.7, 134.2, 133.5, 132.0, 130.9, 130.6, 127.6, 125.4, 124.3, 123.3, 123.1, 122.9, 120.6, 118.8, 116.07, 111.6, 106.1, 60.7, 56.9, 21.8. HRMS (ESI): *m/z* calcd for $[M+H]^+$ $C_{26}H_{26}N_3O_4$ 444.1923; found 444.1956.

4.2.13. N-(2-(5-Chloro-1H-benzo[d]imidazol-2-yl)phenyl)cinnamamide (12 m)

Off-white solid; Yield: 78%, 55 mg; M.p: 244–246 °C; FT-IR (cm^{-1}): 3456.9, 3204.5, 3004.3, 2970.9, 1738.8, 1621.9, 1584.5, 1366.2, 1217.1, 1043.9; ^{1}H NMR (500 MHz, DMSO): δ 13.32 (s, 1H), 13.27 (s, 1H), 8.89 – 8.81 (m, 1H), 8.14 (d, J = 7.8 Hz, 1H), 7.91–7.97 (m, 1H), 7.84 (t, J = 8.0 Hz, 2H), 7.61 (dd, J = 8.7, 4.8 Hz, 1H), 7.54 (m, 1H), 7.52 – 7.45 (m, 3H), 7.40 (dd, J = 8.8, 2.2 Hz, 1H), 7.34–7.27 (m, 1H), 7.23 – 7.13 (m, 1H), 6.94 (d, J = 15.7 Hz, 1H). ^{13}C NMR (125 MHz, DMSO-d_6): δ 164.3, 152.5, 143.3, 140.4, 138.9, 134.3, 132.3, 132.2, 131.5, 131.3, 130.8, 130.7, 130.6, 127.9, 124.0, 123.8, 123.6, 120.7, 115.7, 113.1. HRMS (ESI): *m/z* calcd for $[M+H]^+$ $C_{22}H_{17}ClN_3O$ 374.1060; found 374.1084.

4.2.14. (E)-N-(2-(5-Chloro-1H-benzo[d]imidazol-2-yl)phenyl)-3-(2-ethoxyphenyl)acrylamide (12n)

Off-white solid; Yield: 75%, 50 mg; M.p: 239–241 °C; FT-IR (cm^{-1}): 3456.9, 3225.6, 3016.4, 2970.5, 1738.5, 1535.7, 1366.2, 1217.1, 1047.4; ^{1}H NMR (500 MHz, DMSO-d_6): δ 13.36 (s, 1H), 13.12 (s, 1H), 8.88 (d, J = 7.1 Hz, 1H), 8.14 (d, J = 7.7 Hz, 1H), 8.00 (t, J = 15.4 Hz, 1H), 7.94–7.78 (m, 2H), 7.64–7.49 (m, 2H), 7.42 (t, J = 7.6 Hz, 1H), 7.38–7.26 (m, 2H), 7.13 (d, J = 8.2 Hz, 1H), 7.05 (d, J = 6.6 Hz, 1H), 6.96 (d, J = 15.8 Hz, 1H), 4.19 (d, J = 6.6 Hz, 2H), 1.43 (t, J = 6.7 Hz, 3H). ^{13}C NMR (125 MHz, DMSO-d_6): δ 164.9, 157.7, 152.9, 152.5, 143.5, 141.4, 139.1, 136.7, 134.8, 132.8, 131.9, 131.5, 129.5, 128.0, 123.4, 123.2, 121.2, 120.7, 118.6, 115.6, 113.3, 113.1, 111.7, 64.3, 15.0. HRMS (ESI): m/z calcd for $[M+H]^+$ $C_{24}H_{21}ClN_3O_2$ 418.1322; found 418.1325.

4.2.15. (E)-3-(4-Bromophenyl)-N-(2-(5-chloro-1H-benzo[d]imidazol-2-yl)phenyl)acrylamide (12o)

Off-white solid; Yield: 67%, 48 mg; M.p: 258–260 °C; FT-IR (cm^{-1}): 3456.8, 3265.6, 3016.5, 2970.8, 1738.5, 1631.9, 1586.0, 1366.2, 1217.0, 1059.5; ^{1}H NMR (500 MHz, DMSO-d_6): δ 13.37 (s, 1H), 13.21 (s, 1H), 8.85 (d, J = 6.9 Hz, 1H), 8.15 (d, J = 7.7 Hz, 1H), 8.17–8.11 (m, 1H), 7.81 (s, 2H), 7.74–7.56 (m, 4H), 7.55 (t, J = 7.6 Hz, 1H), 7.40–7.27 (m, 2H), 7.00 (d, J = 15.7 Hz, 1H). ^{13}C NMR (125 MHz, DMSO-d_6): δ 164.3, 152.5, 143.3, 140.4, 138.9, 134.3, 132.4, 132.3, 131.5, 131.3, 130.9, 130.7, 130.6, 127.9, 124.0, 123.8, 123.6, 120.8, 115.7, 113.2. HRMS (ESI): m/z calcd for $[M+H]^+$ $C_{22}H_{16}Br^{81}ClN_3O$ 454.0145; found 454.0146.

4.2.16. (E)-3-(2-Bromo-4,6-dimethoxyphenyl)-N-(2-(5-chloro-1H-benzo[d]imidazol-2-yl)phenyl)acrylamide (12p)

Off-white solid; Yield: 65%, 45 mg; M.p: 190–191 °C; FT-IR (cm^{-1}): 3457.0, 3016.3, 2970.8, 1738.7, 1591.3, 1433.3, 1216.9, 1023.5; ^{1}H NMR (500 MHz, DMSO-d_6): δ 13.29 (s, 1H), 12.45 (s, 1H), 8.65 (m, 1H), 8.33–7.84 (m, 4H), 7.79–7.49 (m, 3H), 7.45–7.17 (m, 2H), 6.79 (m, 1H), 3.88 (s, 6H). ^{13}C NMR (125 MHz, DMSO-d_6): δ 168.0, 151.8, 149.2, 141.9, 139.1, 138.9, 131.6, 128.3, 128.0, 127.7, 126.0, 124.9, 120.9, 120.4, 119.6, 116.8, 116.1, 116.0, 115.7, 110.1, 110.0, 56.5. HRMS (ESI): m/z calcd for $[M+H]^+$ $C_{24}H_{20}Br^{81}ClN_3O_3$ 514.0356; found 514.0364.

4.2.17. (E)-N-(2-(5-Chloro-1H-benzo[d]imidazol-2-yl)phenyl)-3-(4-nitrophenyl)acrylamide (12q)

Yellow solid; Yield: 67%, 47 mg; M.p: 218–220 °C; FT-IR (cm^{-1}): 3454.7, 3016.5, 2970.9, 2920.0, 1738.8, 1694.7, 1621.9, 1584.5, 1366.2, 1206.5, 1092.5; ^{1}H NMR (500 MHz, DMSO-d_6): δ 13.22 (s, 2H), 8.30–8.57 (m, 1H), 8.28–8.14 (m, 3H), 7.99 (d, J = 7.7 Hz, 3H), 7.75–7.66 (m, 2H), 7.57–7.37 (m, 3H), 6.75 (d, J = 15.9 Hz, 1H). ^{13}C NMR (125 MHz, DMSO-d_6): δ 167.3, 148.5, 143.3, 141.7, 141.4, 130.7, 129.7, 128.2, 127.5, 124.8, 124.4, 124.2, 123.6, 119.5, 110.2. HRMS (ESI): m/z calcd for $[M+H]^+$ $C_{22}H_{16}ClN_4O_3$ 419.0911; found 419.0918.

4.2.18. (E)-N-(2-(5-Chloro-1H-benzo[d]imidazol-2-yl)phenyl)-3-(3,4,5-trimethoxyphenyl)acrylamide (12r)

White solid; Yield: 70%, 50 mg; M.p: 239–241 °C; FT-IR (cm^{-1}): 3453.9, 3214.5, 3024.3, 2940.9, 1738.8, 1621.9, 1574.5, 1346.2, 1227.1, 1043.9; ^{1}H NMR (500 MHz, DMSO-d_6): δ 13.37 (s, 1H), 13.19 (s, 1H), 8.84 (d, J = 8.3 Hz, 1H), 8.14 (d, J = 7.8 Hz, 1H), 8.03–7.83 (m, 1H), 7.67 (d, J = 14.8 Hz, 1H),7.61 (s, 1H), 7.55 (t, J = 7.6 Hz, 1H), 7.38–7.27 (m, 2H), 7.14 (s, 2H), 6.93 (d, J = 15.7 Hz, 1H), 3.91 (s, 6H), 3.75 (d, J = 13.9 Hz, 3H). ^{13}C NMR (125 MHz, DMSO-d_6): δ 164.7, 153.6, 152.8, 143.5, 141.5, 139.7, 138.8, 134.9, 132.8, 131.7, 130.6, 127.9, 127.2, 124.0, 123.5, 122.8, 120.8, 118.8, 115.7, 113.4, 111.7, 106.3, 60.6, 56.5. HRMS (ESI): m/z calcd for $[M+H]^+$ $C_{25}H_{23}ClN_3O_4$ 464.1377; found 464.1385.

4.2.19. (E)-3-(2-Ethoxyphenyl)-N-(2-(5-fluoro-1H-benzo[d]imidazol-2-yl)phenyl)acrylamide (12 s)

Off white solid; Yield: 70%, 52 mg; M.p: 190–193 °C; FT-IR (cm^{-1}): 3456.9, 3204.5, 3004.3, 2970.9, 1738.8, 1621.9, 1584.5, 1366.2, 1217.1, 1043.9; ^{1}H NMR (500 MHz, DMSO-d_6): δ 13.35 (s, 1H), 13.17 (s, 1H), 8.88 (s, 1H), 8.19–7.76 (m, 3H), 7.66 (s, 2H), 7.25–7.57 (m, 3H), 7.21–6.91 (m, 3H), 6.53 (d, J = 15.0 Hz, 1H), 4.26–4.05 (m, 2H), 1.53–1.29 (m, 3H). ^{13}C NMR (125 MHz, DMSO-d_6): δ 164.9, 157.5, 143.3, 139.4, 136.8, 132.1, 131.9, 130.5 (d, J = 162.1 Hz), 129.1, 127.9, 127.1, 124.6, 123.3, 123.2 (d, J = 51.2 Hz), 121.2, 121.1, 120.6, 119.7, 119.4, 115.8, 113.0, 110.2, 64.4, 15.1. HRMS (ESI): m/z calcd for $[M+H]^+$ $C_{24}H_{21}FN_3O_2$ 402.1618; found 402.1625.

4.2.20. (E)-N-(2-(5-Fluoro-1H-benzo[d]imidazol-2-yl)phenyl)-3-(3,4,5-trimethoxyphenyl) acrylamide (12 t)

White solid; Yield: 67%, 50 mg; M.p: 279–281 °C; FT-IR (cm^{-1}): 3453.9, 3104.5, 2960.9, 1738.8, 1621.7, 1574.5, 1356.2, 1217.1, 1023.9; ^{1}H NMR (500 MHz, DMSO-d_6): δ 13.31 (s, 1H), 13.23 (s, 1H), 8.84 (d, J = 8.3 Hz, 1H), 8.14 (d, J = 7.6 Hz, 1H), 7.68 (d, J = 15.7 Hz, 2H), 7.54 (t, J = 7.7 Hz, 1H), 7.34–7.17 (m, 3H), 7.14 (s, 2H), 6.93 (d, J = 15.7 Hz, 1H), 3.91 (s, 6H), 3.73 (s, 3H). ^{13}C NMR (125 MHz, DMSO-d_6): δ 164.7, 153.6, 141.5, 139.8, 138.9, 131.3, 130.5, 127.8, 123.5, 122.7, 120.7, 115.9, 106.4, 60.6, 56.5. HRMS (ESI): m/z calcd for $[M+H]^+$ $C_{25}H_{23}FN_3O_4$ 448.1673; found 448.1679.

4.2.21. (E)-3-(2-Ethoxyphenyl)-N-(2-(5-methoxy-1H-benzo[d]imidazol-2-yl)phenyl)acrylamide (12u)

White solid; Yield: 80%, 50 mg; M.p: 282–284 °C; FT-IR (cm^{-1}): 3453.9, 3104.5, 2901.9, 1738.8, 1661.7, 1586.5, 1321.6, 1217.1, 1025.9; ^{1}H NMR (500 MHz, DMSO-d_6): δ 13.34 (s, 1H), 13.09 (s, 1H), 8.88 (s, 1H), 8.13 (s, 1H), 7.98 (, J = 15.0 Hz, 1H), 7.84 – 7.61 (m, 2H), 7.39 (m, 4H), 7.18 – 6.90 (m, 4H), 4.21 (s, 2H), 3.86 (s, 3H), 1.53 – 1.39 (m, 3H); ^{13}C NMR (125 MHz, DMSO-d_6): δ 164.9, 158.1, 157.7, 157.4, 138.9, 138.7, 137.5, 136.3, 134.9, 132.1, 130.7, 129.5, 127.2, 124.6, 123.4, 121.3, 120.6, 119.9, 115.9, 113.1, 112.2, 64.3, 55.9, 15.1. HRMS (ESI): m/z calcd for $[M+H]^+$ $C_{25}H_{24}N_3O_3$ 414.1819; found 414.1814.

4.2.22. (E)-3-(4-Bromophenyl)-N-(2-(5-methoxy-1H-benzo[d]imidazol-2-yl)phenyl)acrylamide (12v)

White solid; Yield: 82%, 55 mg; M.p: 285–286 °C; FT-IR (cm^{-1}): 3456.9, 3124.5, 2901.9, 1738.8, 1631.7, 1566.5, 1331.6, 1227.1, 1025.9; ^{1}H NMR (500 MHz, DMSO-d_6): δ 13.48 (s, 1H), 13.12 (s, 1H), 8.85 (s, 1H), 8.13 (s, 1H), 7.81 (s, 2H), 7.71–7.65 (m, 3H), 7.56–7.41 (m, 2H), 7.31–7.27 (m, 2H), 7.08–6.95 (m, 2H), 3.86 (s, 3H).^{13}C NMR (125 MHz, DMSO-d_6): δ 164.2, 140.0, 138.5, 138.0, 134.2, 132.41, 130.8, 130.8, 130.7, 130.7, 127.1, 124.2, 123.7, 123.6, 120.7, 120.1, 116.2, 112.4, 56.0. HRMS (ESI): m/z calcd for $[M+H]^+$ $C_{23}H_{19}BrN_3O_2$ 447.0582; found 447.0587.

4.3. Biological procedures

4.3.1. Material and Methods:

Human lung cancer cell line (A549) mouse breast cancer cell line (4 T1), human breast cancer cell line (MDA-MB-231), mouse melanoma cell line (B16-F10), human breast cancer cell line (BT-474), normal kidney cell line (NRK-52E) were obtained from National Center for Cell Sciences (NCCS, Pune, India). Cells were cultured in respective (Dulbecco's Modified Eagle's medium) DMEM), RPMI (Roswell Park Memorial Institute medium, Sigma Aldrich, St. Louis, USA) and media was supplemented with 10% fetal bovine serum (FBS) (Gibco, USA) and 1% stabilized antibiotic, penicillin–streptomycin mixture (Gibco, USA). Cells were maintained at 37 °C in a CO_2 incubator with 5% CO_2 and 90% relative humidity. Trypsin-EDTA required for cell culture was obtained from (Gibco, USA). 4′, 6-Diamidino-2-phenylindole (DAPI), fluorescent dyes acridine orange (AO) were from Sigma Aldrich, St.

Louis, USA, while Dichlorofluorescin diacetate (DCFDA) and JC-1 dyes were procured from Invitrogen, USA.

4.3.2. Anticancer activity

Cytotoxic activity of compounds **12a-v** of the series was carried out by (3-(4,5-dimethylthiazol-2-yl)-2,5-diphenyl tetrazolium bromide (MTT) assay. Cells were plated in a 96 well plate at a density of $5x10^3$ cells per well, supplemented with 10% FBS and they were incubated for 24 h at 37 °C in 5% CO_2 later they were treated with the compounds in respective concentrations in the culture media with vehicle controls and known standard (nocodozole). After 48 h of treatment, 100 μL of MTT reagent (0.5 mg/mL) dissolved in serum free media was added to each well and incubated for 4 h. Then the supernatant media was removed carefully, washed with PBS. The formazan crystals formed were dissolved in 200 μL of DMSO and absorbance was taken at 570 nm in multimode plate reader (Spectra Max M4, Molecular devices, US).

4.3.3. Cell morphology by phase contrast imaging

A549 cells were plated with density of $1x10^5$ cells/mL in 24 well culture plates and allowed to adhere by incubating at 37 °C in 5% CO_2 atmosphere for 24 h. Later, cells were incubated with various concentrations of compound **12 h** (0.1, 0.25 and 0.5 μM). After 24 h of incubation with compound **12h**, morphological changes and viability of cells were observed and respective images were captured by using phase contrast microscope (Nikon, Inc. Japan) at 100X magnification.

4.3.4. Acridine orange (AO) staining

Apoptosis induced by the compound **12h** was studied by AO staining, for this, A549 cells were plated with density of $2x10^5$ cells/mL in 24 well plates. After allowing the cells to adhere to plates for overnight, they were treated with different concentrations of compound **12h** (0.1, 0.25 and 0.5 μM) and incubated at 37 °C in an atmosphere of 5% CO_2 for 24 h. For AO staining, 1 mg/mL concentration was added into wells to reach concentration of 10 μg/mL. After 10 min, cells were washed thoroughly and visualized under fluorescence microscope (Nikon, Inc. Japan) with excitation 488 nm and emission 550 nm wavelengths at 100X magnifications and representative images were captured.

4.3.5. DAPI staining

Compound **12h** induced nuclear changes were studied using DAPI staining [27]. Here cells were seeded at the density of $2x10^5$ cells/well and allowed to adhere for overnight. After that cells were incubated with compound **12h** for 24 h. After incubation, cells were washed with PBS and permealised for 5 min with 0.1% Tween 20, later cells were fixed with 4% paraformaldehyde followed by staining with 1 mM DAPI. Fluorescence microscope was used to observe control and treated cells with wavelengths of excitation at 350 nm and emission at 460 nm using DAPI filter at 100X magnifications and representative images were captured.

4.3.6. Measurement of reactive oxygen species (ROS) generation by DCFDA staining

A549 cells were plated at a density of $2x10^5$ cells/mL in 24 well plates and allowed to adhere for overnight. Later, cells were treated with compound **12h** at concentrations of 0.1, 0.25 and 0.5 μM of for 24 h. Then the media was replaced with culture medium containing DCFDA dye (10 mM) and incubated for 30 min in dark. Fluorescence spectroscopy (SpectraMax, Molecular devices) was used to detect the intensity of this fluorescence from cells at an excitation and emission wavelength of 480 and 535 nm, respectively and the corresponding images were captured at 100X magnification.

4.3.7. Measurement of mitochondrial membrane potential by JC-1 staining

A549 cells were cultured in 12 well plates at a density of $5x10^5$ cells/mL and allowed to adhere over night. Next day, cells were treated with compound **12 h** at different concentrations (0.1, 0.25. 0.5 μM) for 24 h, and then cells were incubated with JC-1 stain (2.5 mg/mL) [28] for 30 min. Post incubation, adhered cells were collected by trypsinization, washed with PBS and cells were resuspended in a solution of PBS. Then samples were analyzed for JC-1 fluorescence using flow-cytometer (BD FACSVerseTM, USA).

4.3.8. Scratch wound healing assay

To perform this assay, A549 cells (4×10^5/ well) were seeded in 24 well plates and grown until formation of monolayer. After formation of monolayer, it was wounded with micro pipette tip carefully. Monolayers were washed twice with PBS to remove all the non-adherent cells. Then cells were treated with 0.05, 0.1 and 0.25 μM concentrations of compound **12 h** and cells were allowed to migrate into the wound area. Images of wounds from all the groups were taken at 0 and 24 h post wound induction. After 24 h post treatment, migrated cells were observed and compared with that of the control cells (DMSO treatment), the same was photographed under Carl Zeiss Phase contrast Microscope at 10X objective lens and width was measured using the Zenn software and percentage wound closure was calculated as migration of cancer cells towards the wound or gap'.

4.3.9. Annexin v FITC / propidium iodide binding assay

In order to determine the extent of apoptosis induced cell death annexin V FITC and propidium iodide staining was performed by using the Annexin V FITC apoptosis detection kit according to manufacturer's protocol (Sigma Aldrich). In brief, cells were seeded at a density of 1×10^6 cells per well in 12 well plates and allowed to adhere for overnight. Cells were treated with different concentrations of 0.1, 0.25 and 0.5 μM compounds along with the vehicle control. After 24 h of incubation, cells were harvested, washed with PBS and stained with Annexin V FITC and propidium iodide. Early and late apoptotic cells were quantified using flow cytometer (BD FACSVerse™, USA) based software (BD Biosciences).

4.3.10. Flow cytometry for cell cycle analysis

To examine the effect of **12h** on cell cycle, A549 cells were plated with the density of $1x10^6$/well in 12 well plates for 24 h and then cells were treated with 0.1, 0.25 and 0.5 μM concentrations of compound **12h** for 24 h, and then adhered cells were collected by trypsinisation, washed with PBS (pH 7.4) and fixed. Following fixation, cells were rewashed with PBS and stained with (450 μL) Propidium Iodide (PI) for 15 min in dark at room temperature. The stained samples were then analysed by flow cytometry (BD FACSVerse™, USA). 10,000 events/group were considered for analysing results.

4.3.11. Tubulin polymerization assay

To demonstrate the effect of 12 h on tubulin polymerization, fluorescence based cell free *in vitro* tubulin polymerization assay was performed according to the manufacturer's protocol (BK011, Cytoskeleton, Inc.). The reaction mixture for the experiment contain Porcine brain tissue (2 mg/mL) in 80 mM PIPES pH 6.9, 2.0 mM $MgCl_2$, 0.5 mM EGTA, 1.0 mM GTP and glycerol, experiment was performed in the presence of test compound **12h** (final concentration of 1.25, 2.5, 5.0, 10.0 μM), control and standard (paclitaxel) at 3 μM concentration. Polymerization was monitored by time dependent increase in the fluorescence at 37 °C by a fluorescence reporter incorporated into microtubules. Fluorescence emission at 440 nm (excitation wavelength is 360 nm) was measured by using a spectramax M4 multi-mode micro -plate detection System. The compound concentration required to inhibit 50% of tubulin assembly in comparison to control (IC_{50}) was calculated.

4.3.12. Molecular docking simulation study

The 3D structure of compound **12h** was built on Maestro Molecule Builder of Schrödinger. The built molecule was optimized using OPLS_2005 force field in LigPrep module of Schrödinger 2017–1, Glide

7.4 software [29]. Docking procedure was followed using the standard protocol implemented in Maestro, 11.1 and the compound **12h** was docked against the colchicine binding site of α/β-tubulin interphase (PDB ID: 3E22). The ligand–protein complex was analyzed for interactions and the 3D pose of most active compound **12h** was taken using Schrödinger.

Declaration of Competing Interest

The authors declare that they have no known competing financial interests or personal relationships that could have appeared to influence the work reported in this paper.

Acknowledgements

The authors are thankful to DoP, Ministry of Chemicals & Fertilizers, Govt. of India, for the award of NIPER fellowship. NIPER Research Communication No.: NIPER-H/2020/M004.

Appendix A. Supplementary material

Supplementary data to this article can be found online at https://doi.org/10.1016/j.bioorg.2020.104191.

References

[1] S. Sharma, C. Kaur, A. Budhiraja, K. Nepali, M.K. Gupta, A.K. Saxena, P.M. Bedi, Chalcone based azacarboline analogues as novel antitubulin agents: design, synthesis, biological evaluation and molecular modelling studies, Eur. J. Med. Chem. 85 (2014) 648–660.

[2] A.L. Parker, M. Kavallaris, J.A. McCarroll, Microtubules and their role in cellular stress in cancer, Front. Oncol. 4 (2014) 1–19.

[3] E. Nogales, Structural insights into microtubule function, Annu. Rev. Biochem. 69 (2000) 277–302.

[4] M.A. Jordan, L. Wilson, Microtubules as a target for anticancer drugs, Nat. Rev. Cancer 4 (2004) 253–265.

[5] Y. Lu, J. Chen, M. Xiao, W. Li, D.D. Miller, An overview of tubulin inhibitors that interact with the colchicine binding site, Pharm. Res. 29 (2012) 2943–2971.

[6] (a) A. Kamal, M.d. Ashraf, S.T. Basha, S.M. Ali Hussaini, S. Singh, M.V.P.S. Vishnuvardhan, B. Kiran, B. Sridhar, Design, synthesis and anti-proliferative activity of the new conjugates of E7010 and resveratrol as tubulin polymerization inhibitors, Org. Biomol. Chem. 14 (2016) 1382–1394;
(b) S. Sana, R. Tokala, D.M. Bajaj, K.K. Bokara, G. Kiranmai, U.J. Lakshmi, S. Vadlamani, N. Nagesh, V. Talla, N. Shankaraiah, Design and synthesis of substituted dihydropyrimidinone derivatives as cytotoxic and tubulin polymerization inhibitors, Bioorg. Chem. 93 (2019) 103317;
(c) C. Jadala, M. Satish, P. Anchi, R. Tokala, U.J. Lakshmi, V.G. Reddy, N. Shankaraiah, C. Godugu, A. Kamal, Synthesis of combretastatin-A4 carboxamides mimicking with sulfonyl piperazines by a molecular hybridization approach: In vitro cytotoxicity evaluation and tubulin polymerization inhibition, ChemMedChem 14 (2019) 2052–2060;
(d) N. Shankaraiah, S. Nekkanti, U.R. Brahma, N.P. Kumar, N. Deshpande, D. Prasanna, K.R. Senwar, U.J. Lakshmi, Synthesis of different heterocycles-linked chalcone conjugates as cytotoxic agents and tubulin polymerization inhibitors, Bioorg. Med. Chem. 25 (2017) 4805–4816.

[7] W. Li, H. Sun, S. Xu, Z. Zhu, J. Xu, Tubulin inhibitors targeting the colchicine binding site: a perspective of privileged structures, Future Med. Chem. 9 (2017) 1765–1794.

[8] (a) J.Y. Choi, H. Kim, Y.J. Choi, A. Ishihara, K. Back, S.G. Lee, Cytoprotective activities of hydroxycinnamic acid amides of serotonin against oxidative stress-induced damage in HepG2 and HaCaT cells, Fitoterapia 81 (2010) 1134–1141;
(b) H. Shi, D. Xie, R. Yang, Y. Cheng, Synthesis of caffeic acid phenethyl ester derivatives, and their cytoprotective and neuritogenic activities in PC12 Cells, J. Agric. Food Chem. 62 (2014) 5046–5053;
(c) Y. Miyamae, M. Kurisu, K. Murakami, J. Han, H. Isoda, K. Irie, H. Shigemori, Protective effects of caffeoylquinic acids on the aggregation and neurotoxicity of the 42-residue amyloid β-protein, Bioorg. Med. Chem. 20 (2012) 5844–5849;
(d) T. Takahashi, M. Miyazawa, Synthesis and structure–activity relationships of phenylpropanoid amides of serotonin on tyrosinase inhibition, Bioorg. Med. Chem. Lett. 21 (2011) 1983–1986;
[8] Z. Wu, L. Zheng, Y. Li, F. Su, X. Yue, W. Tang, X. Ma, J. Nie, H. Li, Synthesis and structure–activity relationships and effects of phenylpropanoid amides of octopamine and dopamine on tyrosinase inhibition and antioxidation, Food Chem. 134 (2012) 1128–1131.

[9] C. Pfenning, H.L. Esch, R. Fliege, L. Lehmann, The mycotoxin patulin reacts with DNA bases with and without previous conjugation to GSH: implication for related α, β-unsaturated carbonyl compounds? Arch Toxicol. 90 (2016) 433–448.

[10] N. Sankara Rao, N. Nagesh, V. Lakshma Nayak, S. Sunkari, R. Tokala, P. Gaddam Kiranmai, N. Regur, A.K. Shankaraiah, Design and synthesis of DNA-intercalative naphthalimide-benzothiazole/cinnamide derivatives: cytotoxicity evaluation and topoisomerase-IIα inhibition, Med. Chem. Commun. 10 (2019) 72–79.

[11] P. De, M. Baltas, F. Bedos-Belval, Cinnamic acid derivatives as anticancer agents - a review, Curr. Med. Chem. 18 (2011) 1672–1703.

[12] (a) R.A. Haque, M.A. Iqbal, M.B. Khadeer Ahamed, A.M.S. Abdul Majeed, Z.A.A. Hameed, Design, synthesis and structural studies of meta-xylyl linked bis-benzimidazolium salts: Potential anticanceragents against human colon cancer, Chem. Cent. J. 6 (2012) 1–14;
(b) K. Harkala, L. Eppakayala, T.C. Maringanti, Synthesis and biological evaluation of benzimidazole-linked 1,2,3-triazole congeners as agents, Org. Med. Chem. Lett. 4 (2014) 14–18;
(c) A.A. Rashedy, H.Y. Aboul Enein, Benzimidazole derivatives as potential chemotherapeutic agents, Curr. Drug Ther. 8 (2013) 1–14.

[13] H.A. Barker, R.D. Smyth, H. Weissbach, J.I. Toohey, J.N. Ladd, B.E. Volcani, Isolation and properties of crystalline cobamide coenzymes containing benzimidazole or 5,6- dimethylbenzimidazole, J. Biol. Chem. 235 (1960) 480–488.

[14] (a) A.A. El Rashedy, H.Y. Aboul-Enein, Benzimidazole derivatives as potential anticancer agents, Mini-rev. Med. Chem. 13 (2013) 399–407;
(b) S. Yadav, B. Narasimhan, H. Kaur, Perspectives of benzimidazole derivatives as anticancer agents in the new era, Anti-cancer Agents, Med. Chem. 16 (2016) 1403–1425 38;
(c) N.P. Kumar, P. Sharma, S.S. Kumari, U. Brahma, S. Nekkanti, N. Shankaraiah, A. Kamal, Synthesis of substituted phenanthrene-9-benzimidazole conjugates: Cytotoxicity evaluation and apoptosis inducing studies, Eur. J. Med. Chem. 140 (2017) 128–140.

[15] (a) C. Viegas-Junior, A. Danuello, V. da Silva Bolzani, E.J. Barreiro, C.A. Manssour Fraga, Molecular Hybridization: A useful tool in the design of new drug prototypes, Curr. Med. Chem. 14 (2007) 1829–1852;
(b) N. Shankaraiah, S. Nekkanti, O. Ommi, P.S.L. Soukya, Diverse targeted approaches to battle multidrug resistance in cancer, Curr. Med. Chem. 26 (2019) 7059–7080;
(c) S. Nekkanti, R. Tokala, N. Shankaraiah, Targeting DNA minor groove by hybrid molecules as anticancer agents, Curr. Med. Chem. 24 (2017) 2887–2907.

[16] K. Donthiboinaa, P. Anchi, P.V. Sri Ramya, S. Karri, G. Srinivasulu, C. Godugu, N. Shankaraiah, A. Kamal, Synthesis of substituted biphenyl methylene indolinones as apoptosis inducers and tubulin polymerization inhibitors, Bioorg. Chem. 86 (2019) 210–223.

[17] V. Naidu, U.M. Bandari, A.K. Giddam, K.R.D. Babu, J. Ding, K.S. Babu, B. Ramesh, R.R. Pragada, P. Gopalakrishna, Apoptogenic activity of ethyl acetate extract of leaves of Memecylon edule on human gastric carcinoma cells *via* mitochondrial dependent pathway. Asian Pac, J Trop. Med. 6 (2013) 337–345.

[18] P. Sharma, T.S. Reddy, D. Thummuri, K.R. Senwar, N.P. Kumar, V.G.M. Naidu, S.K. Bhargava, N. Shankaraiah, Synthesis and biological evaluation of new benzimidazole-thiazolidinedione hybrids as potential cytotoxic and apoptosis inducing agents, Eur. J. Med. Chem. 124 (2016) 608–621.

[19] P.V.S. Ramya, L. Guntuku, S. Angapelly, C.S. Digwal, U.J. Lakshmi, D.K. Sigalapalli, B.N. Babu, V.G.M. Naidu, A. Kamal, Synthesis and biological evaluation of curcumin inspired imidazo[1,2-*a*]pyridine analogues as tubulin polymerization inhibitors, Eur. J. Med. Chem. 143 (2018) 216–231.

[20] S. Marchi, C. Giorgi, J.M. Suski, C. Agnoletto, A. Bononi, M. Bonora, E. DeMarchi, S. Missiroli, S. Patergnani, F. Poletti, A. Rimessi, J. Duszynski, M.R. Wieckowski, P. Pinton, Mitochondria-ros crosstalk in the control of cell death and aging, J. Signal Transduct. 2012 (2012) 1–17.

[21] D. Trachootham, J. Alexandre, P. Huang, Targeting cancer cells by ROS mediated mechanisms: a radical therapeutic approach? Nat. Rev. Drug Discov. 8 (2009) 579–591.

[22] A. Nagarsenkar, L. Guntuku, S.D. Guggilapu, K.D. Bai, S. Gannoju, V.G.M. Naidu, B.N. Babu, Synthesis and apoptosis inducing studies of triazole linked 3-benzylidene isatin derivatives, Eur. J. Med. Chem. 124 (2016) 782–793.

[23] (a) B.R. Acharya, S. Bhattacharyya, D. Choudhury, G. Chakrabarti, The microtubule depolymerizing agent naphthazarin induces both apoptosis and autophagy in A549 lung cancer cells, Apoptosis 16 (2011) 924–939;
(b) D. Choudhury, P.L. Xavier, K. Chaudhari, R. John, A.K. Dasgupta, T. Pradeep, Gopal Chakrabarti, Unprecedented inhibition of tubulin polymerization directed by gold nanoparticles inducing cell cycle arrest and apoptosis, Nanoscale 5 (2013) 4476–4489;
(c) M. Liu, X. Zhao, J. Zhao, L. Xiao, H. Liu, C. Wang, L. Cheng, N. Wu, X. Lin, Induction of apoptosis, G0/G1 phase arrest and microtubule disassembly in K562 leukemia Cells by Mere15, a Novel Polypeptide from Meretrix meretrix Linnaeus, Mar. Drugs 10 (2012) 2596–2607.

[24] P.V.S. Ramya, S. Angapelly, L. Guntuku, C.S. Digwal, B.N. Babu, V.G.M. Naidu, A. Kamal, Synthesis and biological evaluation of curcumin inspired indole analogues as tubulin polymerization inhibitors, Eur. J. Med. Chem. 127 (2017) 100–114.

[25] A.H. Shinde, S. Arepally, M.D. Baravkar, D.S. Sharada, Nickel-catalyzed aerobic oxidative isocyanide insertion: access to benzimidazoquinazoline derivatives *via* a sequential double annulation cascade (SDAC) Strategy, J. Org. Chem. 82 (2017) 331–342.

[26] S. Angapelly, P.V. Sri Ramya, A. Angeli, C.T. Supuran and M Arifuddin, Sulfocoumarin-, coumarin-, 4-sulfamoylphenyl-bearing indazole-3-carboxamide hybrids: synthesis and selective inhibition of tumor-associated carbonic anhydrase isozymes IX and XII. ChemMedChem 12 (19) 1578-1584.

[27] N.P. Kumar, S. Thatikonda, R. Tokala, S.S. Kumari, U.J. Lakshmi, G. Chandraiah, N. Shankaraiah, A. Kamal, Sulfamic acid promoted one-pot synthesis of phenanthrene fused-dihydrodibenzo-quinolinones: Anticancer activity, tubulin polymerization inhibition and apoptosis inducing studies, Bioorg. Med. Chem. 26 (2018) 1996–2008.

[28] R. Tokala, S. Bale, I.P. Janrao, A. Vennela, N.P. Kumar, K.R. Senwar, G. Chandraiah, N. Shankaraiah, Synthesis of 1,2,4-triazole-linked urea/thiourea conjugates as cytotoxic and apoptosis inducing agents, Bioorg. Med. Chem. Lett. 28 (2018) 1919–1924.

[29] Schrödinger Suite 2017-1, Schrödinger, LLC, New York (2017).